

# Grain Growth, Sintering, and Vitrification

We have previously discussed phase changes, polymorphic transformations, and other processes independent of, or subsequent to, the fabrication of ceramic bodies. Phenomena that are of great importance are the processes taking place during heat treatment before use; these are the subject of this chapter.

During the usual processing of ceramics, crystalline or noncrystalline powders are compacted and then fired at a temperature sufficient to develop useful properties. During the firing process changes may occur initially because of decomposition or phase transformations in some of the phases present. On further heating of the fine-grained, porous compact, three major changes commonly occur. There is an increase in grain size; there is a change in pore shape; there is change in pore size and number, usually to give a decreased porosity. In many ceramics there may be solid-state reactions forming new phases, polymorphic transformations, decompositions of crystalline compounds to form new phases or gases, and a variety of other changes which are frequently of great importance in particular cases but are not essential to the main stream of events.

We shall be mainly concerned with developing an understanding of the major processes taking place. There are so many things which can happen, and so many variables that are occasionally important, that no mere cataloging of phenomena can provide a sound basis for further study. In general, we shall be concerned first with recrystallization and grain-growth phenomena, second with the densification of single-phase systems, and finally with more complex multiphase processes. There are many important practical applications for each of these cases.

## 10.1 Recrystallization and Grain Growth

The terms recrystallization and grain growth have had a very broad and indefinite usage in much of the ceramic literature; they have sometimes been used to include phase changes, sintering, precipitation, exsolution, and other phenomena which produce changes in the microstructure. We are mainly concerned with three quite distinct processes. *Primary recrystallization* is the process by which nucleation and growth of a new generation of strainfree grains occurs in a matrix which has been plastically deformed. *Grain growth* is the process by which the average grain size of strainfree or nearly strainfree material increases continuously during heat treatment without change in the grain-size distribution. *Secondary recrystallization*, sometimes called abnormal or discontinuous grain growth, is the process by which a few large grains are nucleated and grow at the expense of a fine-grained, but essentially strain-free, matrix. Although all these processes occur in ceramic materials, grain growth and secondary recrystallization are the ones of major interest.

**Primary Recrystallization.** This process has as its driving force the increased energy of a matrix which has been plastically deformed. The energy stored in the deformed matrix is of the order of 0.5 to 1 cal/g. Although this is small compared with the heat of fusion, for example (which is a 1000 or more times this value), it provides a sufficient energy change to effect grain-boundary movement and changes in grain size.

If the isothermal change in grain size of strainfree crystals in a deformed matrix is measured after an initial induction period, there is a constant rate of grain growth for the new strainfree grains. If the grain size is  $d$ ,

$$d = U(t - t_0) \quad (10.1)$$

where  $U$  is the growth rate (cm/sec),  $t$  is the time, and  $t_0$  is the induction period. This is illustrated in Fig. 10.1 for recrystallization of a sodium chloride crystal which had been deformed at 400°C and then annealed at 470°C. The induction period corresponds to the time required for a nucleation process, so that the overall rate of recrystallization is determined by the product of a nucleation rate and a growth rate.

The nucleation process is similar to those discussed in Chapter 8. For a nucleus to be stable, its size must be larger than some critical diameter at which the lowered free energy of the new grain is equal to the increased surface free energy. The induction period corresponds to the time required for unstable embryos present to grow to the size of a stable nucleus. If an unlimited number of sites is available, the rate of nucleation increases to some constant rate after an initial induction period. In

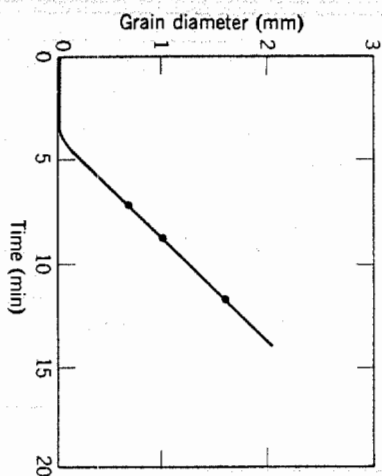


Fig. 10.1. Recrystallization of NaCl deformed at 400°C (stress = 4000 g/mm<sup>2</sup>) and recrystallized at 470°C. From H. G. Müller, *Z. Phys.*, 96, 279 (1935).

practice the number of favorable sites available is limited, and the rate of nucleation passes through a maximum as they are used up. H. G. Müller\* observed that nuclei in sodium chloride tended to form first at grain corners, for example. As the temperature is increased, the rate of nucleation increases exponentially:

$$\frac{N}{dt} = N_0 \exp \left( -\frac{\Delta G_N}{RT} \right) \quad (10.2)$$

where  $N$  is the number of nuclei and  $\Delta G_N$  is the experimental free energy for nucleation. Consequently, the induction period,  $t_0 \sim 1/(dN/dt)$ , decreases rapidly as the temperature level is raised.

As indicated in Eq. 10.1, the growth rate remains constant until the grains begin to impinge on one another. The constant in growth rate results from the constant driving force (equal to the difference in energy between the strained matrix and strainfree crystals). The final grain size is determined by the number of nuclei formed, that is, the number of grains present when they finally impinge on one another. The atomistic process necessary for grain growth is the jumping of an atom from one side of a boundary to the other and is similar to a diffusional jump in the boundary. Consequently the temperature dependence is similar to that of diffusion:

$$U = U_0 \exp \left( -\frac{E_u}{RT} \right) \quad (10.3)$$

where the activation energy  $E_u$  is normally intermediate between that for boundary and lattice diffusion. The growth-rate-temperature curve for

recrystallization of sodium chloride has a knee similar to that observed for diffusion and conductivity data, as discussed in Chapter 6.

Since both the nucleation rate and the growth rate are strongly temperature-dependent, the overall rate of recrystallization changes rapidly with temperature. For a fixed holding time, experiments at different temperatures tend to show either little or nearly complete recrystallization. Consequently, it is common to plot data as the amount of cold work or the final grain size as a function of the *recrystallization temperature*. Since the final grain size is limited by impingement of the grains on one another, it is determined by the relative rates of nucleation and growth. As the temperature is raised, the final grain size is larger, since the growth rate increases more rapidly than the rate of nucleation. However, at higher temperatures recrystallization is completed more rapidly, so that the larger grain size observed in constant-time experiments (Fig. 10.2) may be partly due to the greater time available for grain growth following recrystallization. The growth rate increases with increasing amounts of plastic deformation (increased driving force), whereas the final grain size decreases with increasing deformation.

In general, it is observed that (1) some minimum deformation is required for recrystallization, (2) with a small degree of deformation a higher temperature is required for recrystallization to occur, (3) an increased annealing time lowers the temperature of recrystallization, and

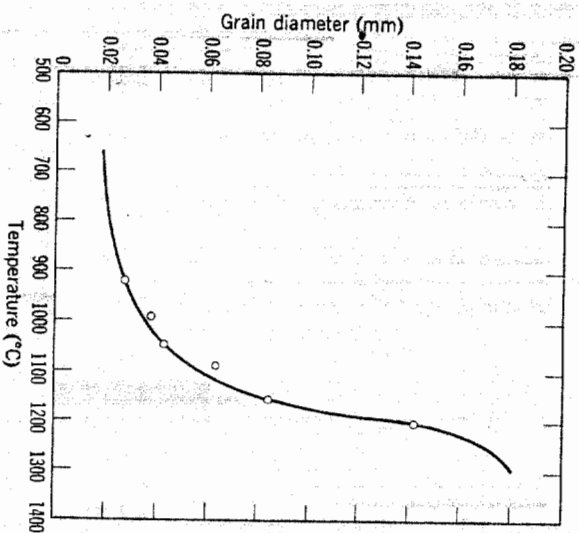


Fig. 10.2. Effect of annealing temperature on grain size of CaF<sub>2</sub> following compression at 80,000 psi and 10 hr at temperature. From M. J. Bueger, *Am. Mineral.*, 32, 296 (1947).

\**Z. Phys.*, 96, 279 (1935).

(4) the final grain size depends on the degree of deformation, the initial grain size, and the temperature of recrystallization. In addition, continued heat after recrystallization is completed leads to the continuation of grain growth.

Primary recrystallization is particularly common in metals which are extensively deformed in normal processing techniques. Ceramic materials are seldom plastically deformed during processing, so that primary recrystallization is not commonly observed. For relatively soft materials, such as sodium chloride or calcium fluoride, deformation and primary recrystallization do occur. It has also been observed directly in magnesium oxide; also, the polygonization process described in Chapter 4 (see Fig. 4.24) for aluminum oxide has many points of similarity.

**Grain Growth.** Whether or not primary recrystallization occurs, an aggregate of fine-grained crystals increases in average grain size when heated at elevated temperatures. As the average grain size increases, it is obvious that some grains must shrink and disappear. An equivalent way of looking at grain growth is as the rate of disappearance of grains. Then the driving force for the process is the difference in energy between the fine-grained material and the larger-grain-size product resulting from the decrease in grain-boundary area and the total boundary energy. This energy change corresponds to about 0.1 to 0.5 cal/g for the change from a 1-micron to a 1-cm grain size.

As discussed in Chapter 5, an interface energy is associated with the boundary between individual grains. In addition, there is a free-energy difference across a curved grain boundary which is given by

$$\Delta G = \gamma \bar{V} \left( \frac{1}{r_1} + \frac{1}{r_2} \right) \quad (10.4)$$

where  $\Delta G$  is the change in free energy on going across the curved interface,  $\gamma$  is the boundary energy,  $\bar{V}$  is the molar volume, and  $r_1$  and  $r_2$  are the principal radii of curvature. (This relationship has been derived and discussed in Chapter 5. That part of Chapter 5 should be reviewed if its meaning is not clear.) This difference in the free energy of material on the two sides of a grain boundary is the driving force that makes the boundary move toward its center of curvature. The rate at which a boundary moves is proportional to its curvature and to the rate at which atoms can jump across the boundary.

Grain growth provides an opportunity to apply the absolute-reaction-rate theory already discussed in Chapter 6. If we consider the structure of a boundary (Fig. 10.3), the rate of the overall process is fixed by the rate at which atoms jump across the interface. The change in energy with an atom's position is shown in Fig. 10.3b, and the frequency of atomic jumps

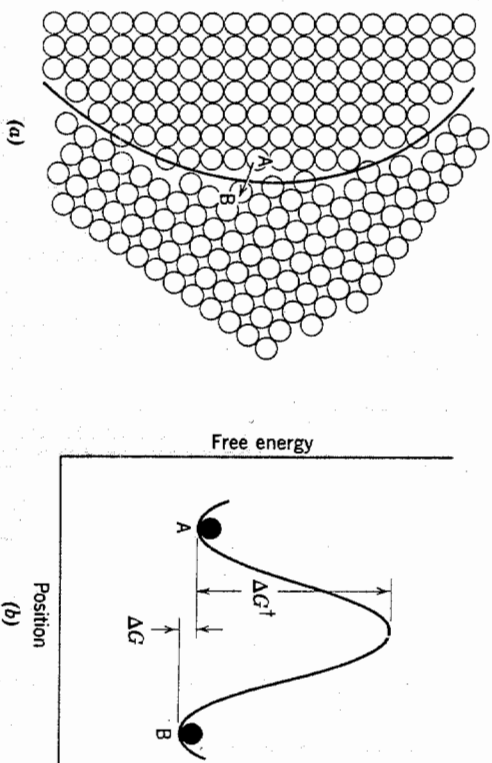


Fig. 10.3. (a) Structure of boundary and (b) energy change for atom jump.

in the forward direction is given by

$$f_{AB} = \frac{RT}{Nh} \exp \left( -\frac{\Delta G^\ddagger}{RT} \right) \quad (10.5)$$

and the frequency of reverse jumps is given by

$$f_{BA} = \frac{RT}{Nh} \exp \left( -\frac{\Delta G^\ddagger + \Delta G}{RT} \right) \quad (10.6)$$

so that the net growth process,  $U = \lambda f$ , where  $\lambda$  is the distance of each jump is given by

$$U = \lambda f = \lambda (f_{AB} - f_{BA}) = \frac{RT}{Nh} (\lambda) \exp \left( -\frac{\Delta G^\ddagger}{RT} \right) \left( 1 - \exp \frac{\Delta G}{RT} \right) \quad (10.7)$$

and since  $1 - \exp \frac{\Delta G}{RT} \approx \frac{\Delta G}{RT}$ , where  $\Delta G = \gamma \bar{V} \left( \frac{1}{r_1} + \frac{1}{r_2} \right)$  and  $\Delta G^\ddagger = \Delta H^\ddagger - T \Delta S^\ddagger$ ,

$$U = \left( \frac{RT}{Nh} \right) (\lambda) \left[ \frac{\gamma \bar{V}}{RT} \left( \frac{1}{r_1} + \frac{1}{r_2} \right) \right] \exp \frac{\Delta S^\ddagger}{R} \exp \left( -\frac{\Delta H^\ddagger}{RT} \right) \quad (10.8)$$

which is equivalent in form to Eq. 10.3 given previously. That is, the rate of growth increases exponentially with temperature. The unit step involved is the jump of an atom across the boundary, so that the activation energy should correspond approximately to the activation energy for boundary diffusion.

If all the grain boundaries are equal in energy, they meet to form angles of  $120^\circ$ . If we consider a two-dimensional example for illustrative purposes, angles of  $120^\circ$  between grains with straight sides can occur only for six-sided grains. Grains with fewer sides have boundaries that are concave when observed from the center of the grain. Shapes of grains having different numbers of sides are illustrated in Fig. 10.4; a sample with uniform grain size is shown in Fig. 10.5. Since grain boundaries migrate toward their center of curvature, grains with less than six sides tend to grow smaller, and grains with more than six sides tend to grow larger. For any one grain, the radius of curvature of a side is directly proportional to the grain diameter, so that the driving force, and therefore the rate of grain growth, is inversely proportional to grain size:

$$\dot{d} = \frac{d(d)}{dt} = \frac{k}{d} \quad (10.9)$$

and integrating,

$$d - d_0 = (2k)^{1/2} t^{1/2} \quad (10.10)$$

where  $d_0$  is the grain diameter at time zero. Experimentally it is found that when  $\log d$  is plotted versus  $\log t$ , a straight line is obtained (Fig. 10.6). Frequently the slope of curves plotted in this way is smaller than one-half.

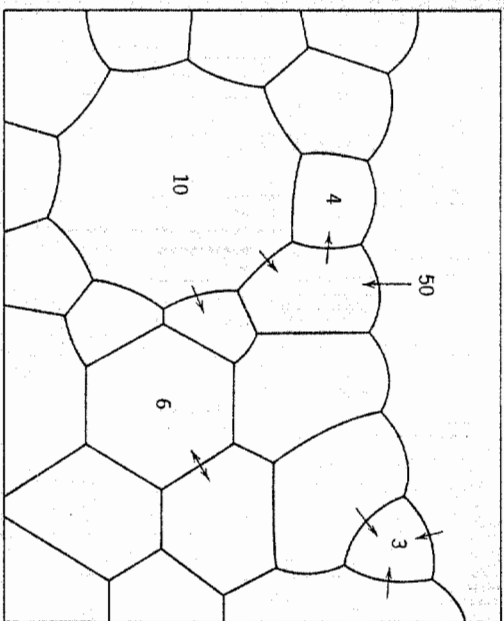


Fig. 10.4. Schematic drawing of polycrystalline specimen. The sign of curvature of the boundaries changes as the number of sides increases from less than six to more than six, and the radius of curvature is less, the more the number of sides differs from six. Arrows indicate the directions in which boundaries migrate. From J. E. Burke.

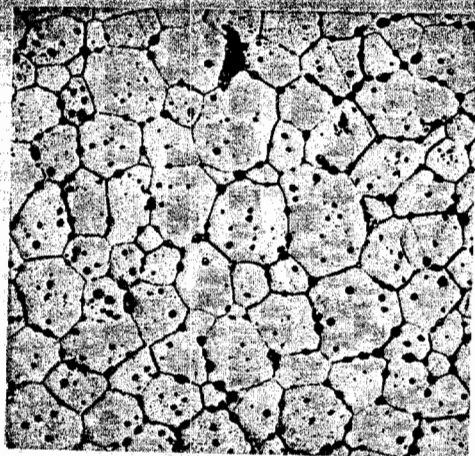


Fig. 10.5. Polycrystalline  $\text{CaF}_2$  illustrating normal grain growth. Average angle at grain junctures is  $120^\circ$ .

usually falling between 0.1 and 0.5. This may occur for several reasons, one being that  $d_0$  is not a large amount smaller than  $d$ ; another common reason is that inclusions or solute segregation or sample size inhibits grain growth.

A somewhat different approach is to define a grain-boundary mobility  $B$ , such that the boundary velocity  $v$  is proportional to the applied driving force  $F$ , resulting from boundary curvature:

$$v = BF_i \quad (10.11a)$$

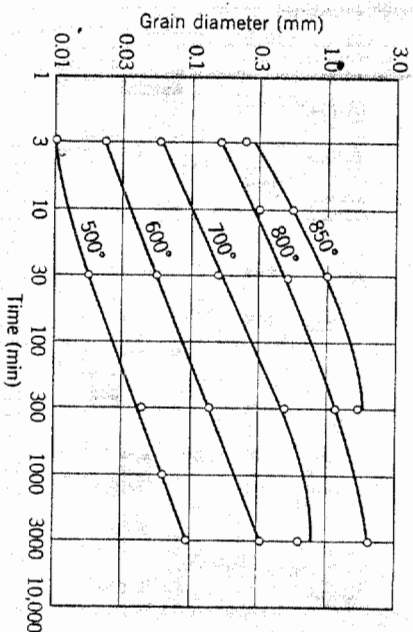


Fig. 10.6. Log grain diameter versus log time for grain growth in pure  $\alpha$ -brass. From J. E. Burke.

For the atomic-jump mechanism illustrated in Fig. 10.3, the boundary mobility is given by the atomic mobility divided by the number of atoms involved,  $n_a$ :

$$B_i = \frac{B_a}{n_a} = \left( \frac{D_b}{kT} \right) \left( \frac{\Omega}{S w} \right), \quad (10.11b)$$

where  $D_b$  is the grain-boundary diffusion coefficient,  $\Omega$  is the atomic volume,  $S$  is the boundary area, and  $w$  is the boundary width. Since the average boundary velocity is equal to  $v$  and the driving force is inversely proportional to grain size, a grain-growth law of the form of Eqs. 10.9 and 10.10 results. However, as discussed in Chapter 5, the actual structure of a ceramic grain boundary is not quite so simple as pictured in deriving Eqs. 10.8 and 10.11b. Even for a completely pure material there is a space-charge atmosphere of lattice defects associated with the boundary and usually solute segregation as well, as shown in Figs. 5.11, 5.12, 5.17, and 5.18. The effect of this lattice defect and impurity atmosphere is to sharply reduce the grain-boundary velocity at low driving forces, as shown in Fig. 10.7 and analysed by J. Cahn\* and K. Lücke and H. JD. Stuwe.† The influence of this atmosphere becomes stronger as the grain

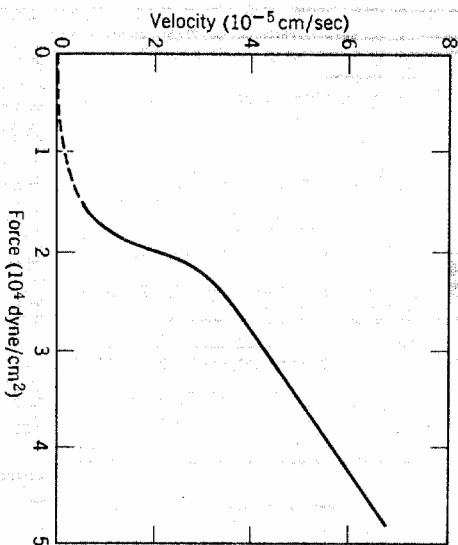


Fig. 10.7. Variation of boundary velocity  $v$  with driving force  $F$  at 750°C for a 20° tilt boundary in NaCl. From R. C. Sun and C. L. Bauer, *Acta Met.*, 18, 639 (1970).

size increases, the solute segregate concentration increases, and the average boundary curvature decreases. Additions of  $MgO$  to  $Al_2O_3$ ,  $CaCl_2$ ,

\* *Acta Met.*, 10, 789 (1962).

† *Acta Met.*, 19, 1087 (1971).

to KCl and of  $ThO_2$  to  $Y_2O_3$  in amounts below the solubility limit have proved effective as grain-growth inhibitors.

When grains grow to such a size that they are nearly equal to the specimen size, grain growth is stopped. In a rod sample, for example, when the grain size is equal to the rod diameter, the grain boundaries tend to form flat surfaces normal to the axis so that the driving force for boundary migration is eliminated and little subsequent grain growth occurs. Similarly, inclusions increase the energy necessary for the movement of a grain boundary and inhibit grain growth. If we consider a boundary such as the one illustrated in Fig. 10.8, the boundary energy is decreased when it reaches an inclusion proportional to the cross-sectional area of the inclusion. The boundary energy must be increased again to pull it away from the inclusion. Consequently, when a number of inclusions are present on a grain boundary, its normal curvature becomes insufficient for continued grain growth after some limiting size is reached. It has been found that this size is given by

$$d_i \approx \frac{d_i}{f_a} \quad (10.12)$$

where  $d_i$  is the limiting grain size,  $d_i$  is the particle size of the inclusion, and  $f_a$  is the volume fraction of inclusions. Although this relationship is only approximate, it indicates that the effectiveness of inclusions increases as their particle size is lowered and the volume fraction increases. For the process illustrated in Fig. 10.8, the boundary approaches, is attached to, and subsequently breaks away from a second-phase particle. Another possibility is that the grain boundary drags along the particle

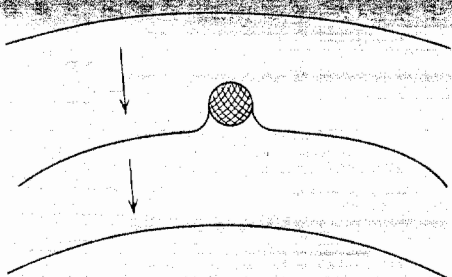


Fig. 10.8. Changing configuration of a boundary while passing an inclusion.

which remains attached to the boundary as it moves. This requires material transport across the particle, which may occur by interface or surface or volume diffusion, by viscous flow, or by solution (precipitation in a liquid or glass inclusion), or by evaporation (condensation in a gas inclusion). We can define an inclusion particle mobility  $B_p$ , relating the driving force and particle velocity  $v_p = B_p F_p$ , in the same way as has been done for the boundary (Eq. 10.11b) and for atomic diffusion in Chapter 6. When the inclusion is dragged by the boundary, their velocities are identical; in the case in which  $B_p \ll B_b$  we can neglect the intrinsic boundary mobility, and the resulting grain-boundary velocity is controlled by the driving force on the boundary together with the mobility and number of inclusions per grain boundary,  $p$ :

$$v_b = \frac{B_p F_b}{p} \quad (10.13)$$

The inclusion particle moves along with the boundary, gradually becoming concentrated at boundary intersections and agglomerating into larger particles as grain growth proceeds. This is illustrated for the special case of pore agglomeration in Figs. 10.9 and 10.10.

Thus, second-phase inclusions can either (1) move along with boundaries, offering little impedance; (2) move along with boundaries, with the inclusion mobility controlling the boundary velocity; or (3) be so immobile that the boundary pulls away from the inclusion, depending on the relative values of the boundary driving force (inversely proportional to grain size), the boundary mobility (Fig. 10.7), and the inclusion particle mobility, which, depending on the assumed mechanism and particle shape, may be proportional to  $r_p^{-2}$ ,  $r_p^{-3}$ , or  $r_p^{-4}$ .\* As grain growth proceeds, the driving force diminishes, and any inclusions dragged along by the boundary increase in size so that their mobility decreases. As a result, the exact way in which second-phase inclusions inhibit grain growth not only depends on the properties of the particular system but also can easily change during the grain-growth process. Sorting out these effects requires a careful evaluation of the microstructure evolution in combination with the kinetics of grain growth and a detailed knowledge of system properties. Inhibition of grain growth by solid second-phase inclusions has been observed for MgO additions to  $Al_2O_3$ , for CaO additions to  $ThO_2$ , and in other systems.

A second phase that is always present during ceramic sintering and in almost all ceramic products prepared by sintering is residual porosity

\*P. G. Shewmon, *Trans. A.I.M.E.*, **230**, 1134 (1964); M. F. Ashby and R. M. A. Cantamore, *Acta Met.*, **16**, 1081 (1968).

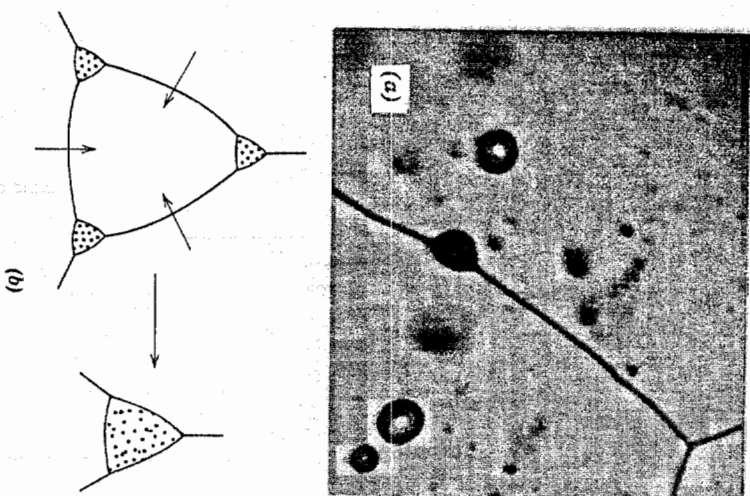


Fig. 10.9. (a) Pore shape distorted from spherical by moving boundary and (b) pore agglomeration during grain growth.

remaining from the interparticle space present in the initial powder compact. This porosity is apparent both on the grain boundaries (intergranular) and within the grains (intragranular) in the sintered  $CaF_2$  sample shown in Fig. 10.5. It is present almost entirely at the grain corners (intergranular) in the sintered  $UO_2$  samples shown in Fig. 10.10. As with particulate inclusions, pores on the grain boundaries may be left behind by the moving boundary or migrate with the boundary, gradually agglomerating at grain corners, as illustrated in Figs. 10.9 and 10.10. In the early stages of sintering, when the boundary curvature and the driving force for boundary migration are high, pores are often left behind, and a cluster of small pores in the center of a grain is a commonly observed result (see Fig. 10.5). In the later stages of sintering, when the grain size is larger and the driving force for boundary migration is lower, it is more usual for pores to be dragged along by the boundary, slowing grain growth.

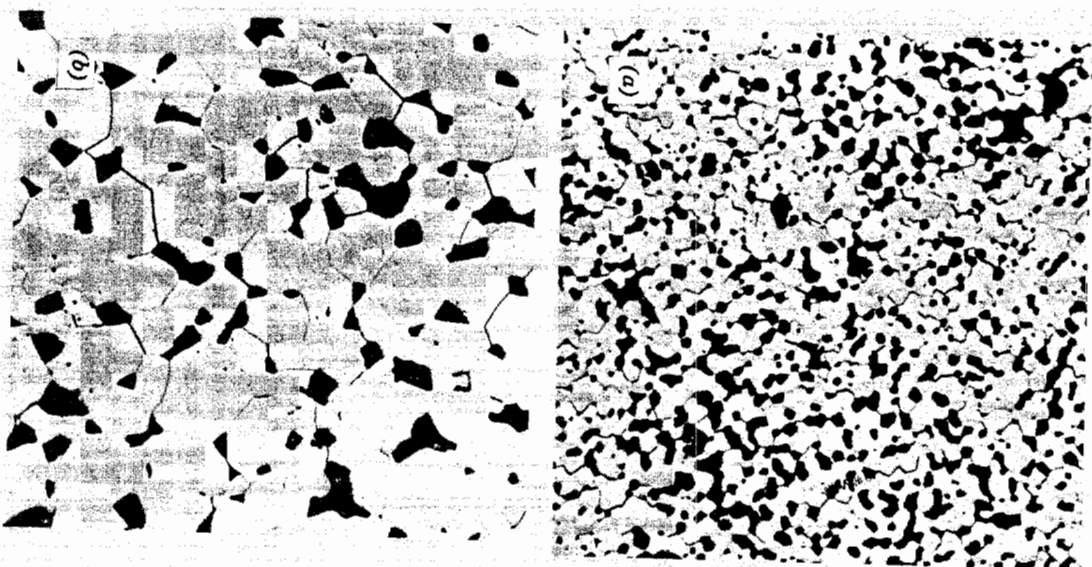


Fig. 10.10. Grain growth and pore growth in sample of  $\text{UO}_2$  after (a) 2 min, 91.5% dense, and (b) 5 hr, 91.9% dense, at  $1600^\circ\text{C}$  ( $400\times$ ). From Francois and Kingery.

Another factor that may restrain grain growth is the presence of a liquid phase. If a small amount of a boundary liquid is formed, it tends to slow grain growth, since the driving force is reduced and the diffusion path is increased. There are now two solid-liquid interfaces, and the driving force is the difference between them, that is,  $(1/r_1 + 1/r_2)_\lambda - (1/r_1 + 1/r_2)_B$ , which

is smaller than either alone; in addition, if the liquid wets the boundary, the interface energy must be lower than the pure-grain-boundary energy. Also, the process of solution, diffusion through a liquid film, and precipitation is usually slower than the jump across a boundary. However, this case is more complex in that grain growth may be enhanced by the presence of a reactive liquid phase during the densification process, as discussed in Section 10.4. In addition, a very small amount of liquid may enhance secondary recrystallization, as discussed later, whereas larger amounts of liquid phase may give rise to the grain-growth process described in Chapter 9. In practice, it is found that addition of a moderate amount of silicate liquid phase to aluminum oxide prevents the extensive grain growth which frequently occurs with purer materials.

**Secondary Recrystallization.** The process of secondary recrystallization, sometimes called discontinuous or exaggerated grain growth, occurs when some small fraction of the grains grow to a large size, consuming the uniform-grain-size matrix. Once a single grain grows to such a size that it has many more sides than the neighboring grains (such as the grain with fifty sides illustrated in Fig. 10.4), the curvature of each side increases, and it grows more rapidly than the smaller grains with fewer sides. The increased curvature on the edge of a large grain is particularly evident in Fig. 10.11, which shows a large alumina crystal growing at the expense of a uniform-particle-size matrix.

Secondary crystallization is particularly likely to occur when continuous grain growth is inhibited by the presence of impurities or pores. Under these conditions the only boundaries able to move are those with a curvature much larger than the average; that is, the exaggerated grains with highly curved boundaries are able to grow, whereas the matrix material remains uniform in grain size. The rate of growth of the large grains is initially dependent on the number of sides. However, after growth has reached the point at which the exaggerated grain diameter is much larger than the matrix diameter,  $d_g \gg d_m$ , the curvature is determined by the matrix grain size and is proportional to  $1/d_m$ . That is, there is an induction period corresponding to the increased growth rate and the formation of a grain large enough to grow at the expense of the constant-grain-size matrix. Therefore, the growth rate is constant as long as the grain size of the matrix remains unchanged. Consequently, the kinetics of secondary recrystallization is similar to that of primary recrystallization, even though the nature of the nucleation and driving force is different.

Secondary recrystallization is common for oxide, titanate, and ferrite ceramics in which grain growth is frequently inhibited by minor amounts of second phases or by porosity during the sintering process. A typical resultant structure is illustrated for barium titanate in Fig. 10.12, and the

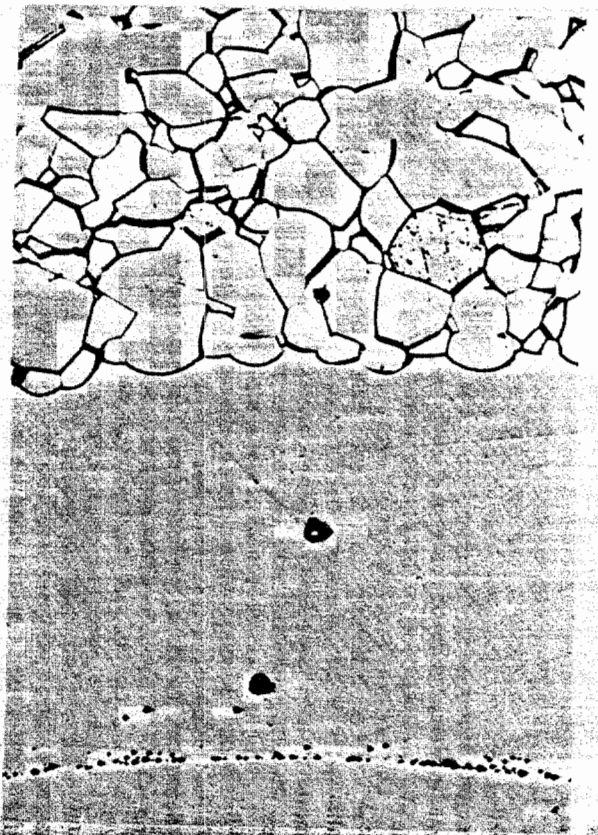


Fig. 10.11. Growth of a large  $\text{Al}_2\text{O}_3$  crystal into a matrix of uniformly sized grains (495 $\times$ ). Compare with Fig. 10.4. Courtesy R. L. Coble.

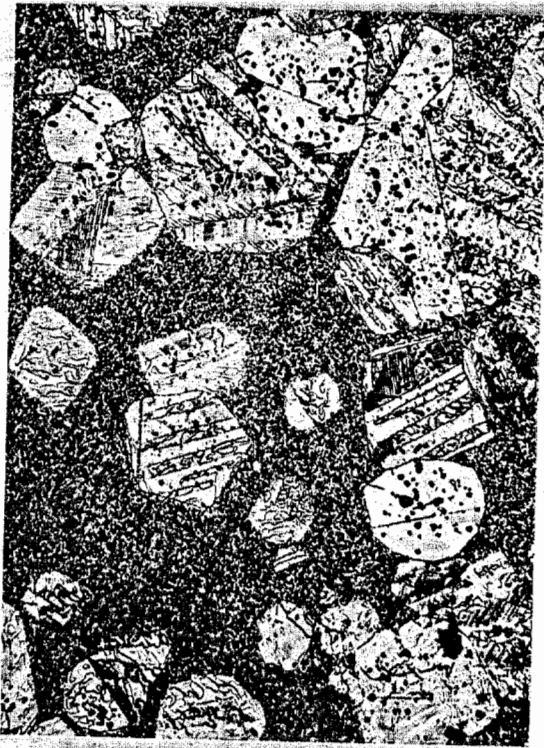


Fig. 10.12. Large grains of barium titanate growing by secondary recrystallization from a fine-grained matrix (250 $\times$ ). Courtesy R. C. DeVries.

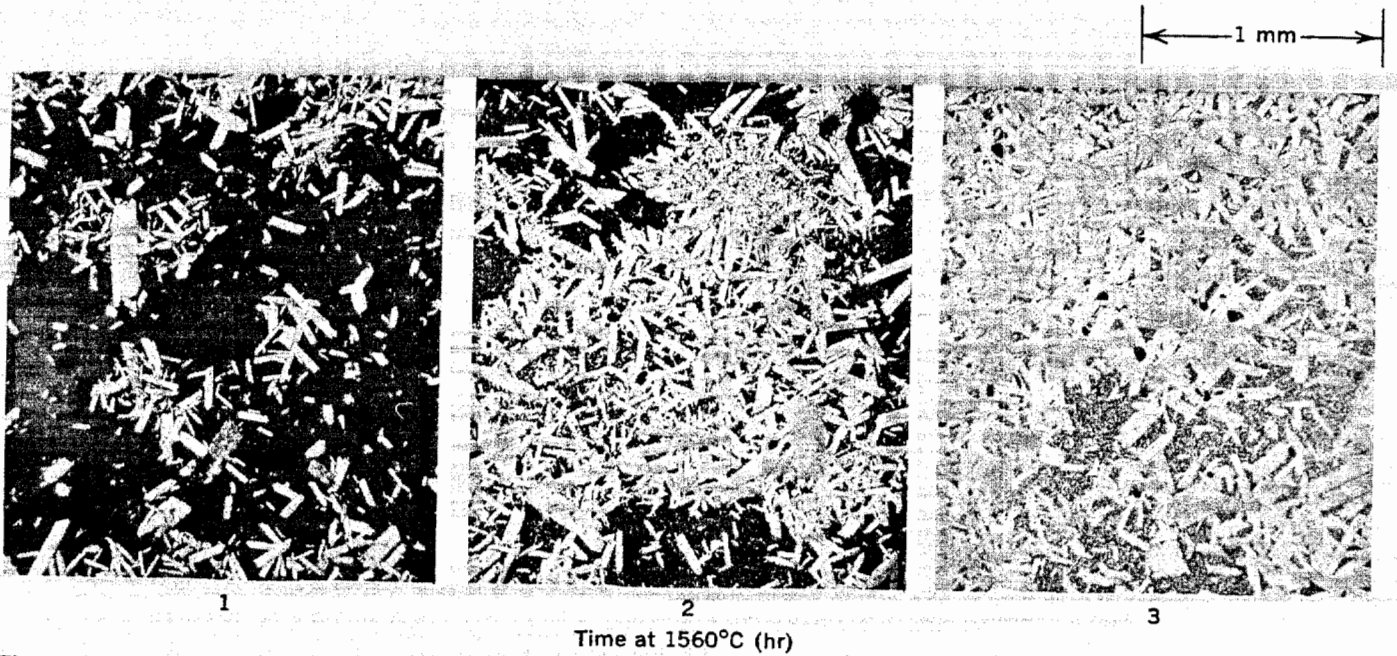


Fig. 10.13. Large grains of  $\text{Al}_2\text{O}_3$  growing by secondary recrystallization from a fine-grained matrix. Courtesy I. B. Cutler, in reference 5.

progressive growth of aluminum oxide crystals during secondary recrystallization is illustrated in Fig. 10.13.

When polycrystalline bodies are made from fine powder, the extent of secondary recrystallization depends on the particle size of the starting material. Coarse starting material gives a much smaller relative grain growth, as illustrated in Fig. 10.14 for beryllia. This is caused by both the rate of nucleation and the rate of growth. There are almost always present in the fine-grained matrix a few particles of substantially larger particle size than the average; these can act as embryos for secondary recrystallization, since already  $d_s > d_m$ , and growth proceeds to a rate proportional to  $1/d_m$ . In contrast, as the starting particle size increases, the chances of grains being present which are much larger in particle size than the average are much decreased, and consequently the nucleation of secondary recrystallization is much more difficult; the growth rate, proportional to  $1/d_m$ , is also smaller. In the data shown in Fig. 10.14, material having a starting particle size of 2 microns grows to a final particle size of about 50 microns, whereas material with an initial particle size of 10 microns shows a final grain size of only about 25 microns. This result of a much larger final grain size for a smaller initial particle size would be very puzzling if the process of secondary recrystallization was not known to occur.

Secondary recrystallization has been observed to occur with the boundaries of the large grains apparently perfectly straight (Fig. 10.15). Here the previous discussion of the surface tension and curvature of the phase boundary does not apply directly. That is, the boundary energy is

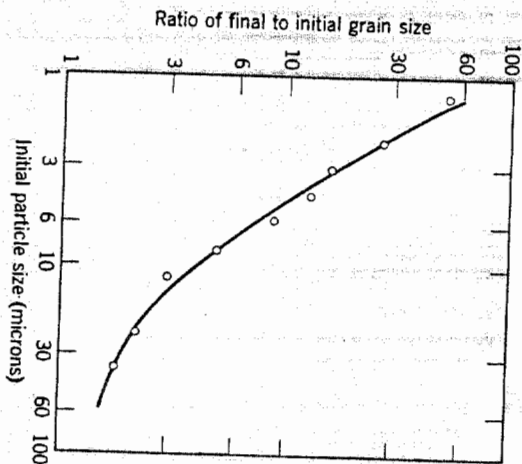


Fig. 10.14. Relative grain growth during secondary recrystallization of BeO heated 24 hr at 2000°C. From P. Duwez, F. Odell, and J. L. Taylor, *J. Am. Ceram. Soc.*, 32, 1 (1949).

not independent of crystal directions, and the growth planes are those of low surface energy. These structures all seem to occur in systems having a small concentration of impurity which gives rise to a small amount of a boundary phase. The driving force for secondary recrystallization is the lower surface energy of the large grain compared with the high-surface-energy faces or small radius of curvature of adjacent grains. Transfer of material under these conditions can only occur when there is an intermediate boundary phase separating the surfaces of the small and large grains. The amount of second phase present tends to increase at the boundaries of the large crystals compared with that at other boundaries in the system, and a large grain continues to grow once it is initiated. If the amount of boundary phase is increased, however, normal grain growth and this kind of secondary recrystallization are both inhibited, as discussed previously.

Secondary recrystallization affects both the sintering of ceramics and resultant properties. Excessive grain growth is frequently harmful to mechanical properties (see Sections 5.5 and 15.5). For some electrical and magnetic properties either a large or a small grain size may contribute to improved properties. Occasionally grain growth has been discussed in the literature as if it were an integral part of the densification process. That this is not true can best be seen from Fig. 10.16. A sample of aluminum oxide with an initial fine pore distribution was heated to a high temperature so that secondary recrystallization occurred. The recrystallization has left almost the same amount of porosity as was present in the initial

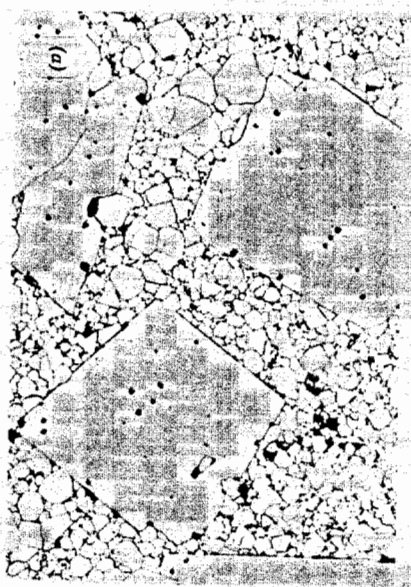


Fig. 10.15. (a) Idiomorphic grains in a polycrystalline spinel. The large grain edges appear straight, whereas the shape of the small grains is controlled by surface tension (350×). Courtesy R. L. Coble.

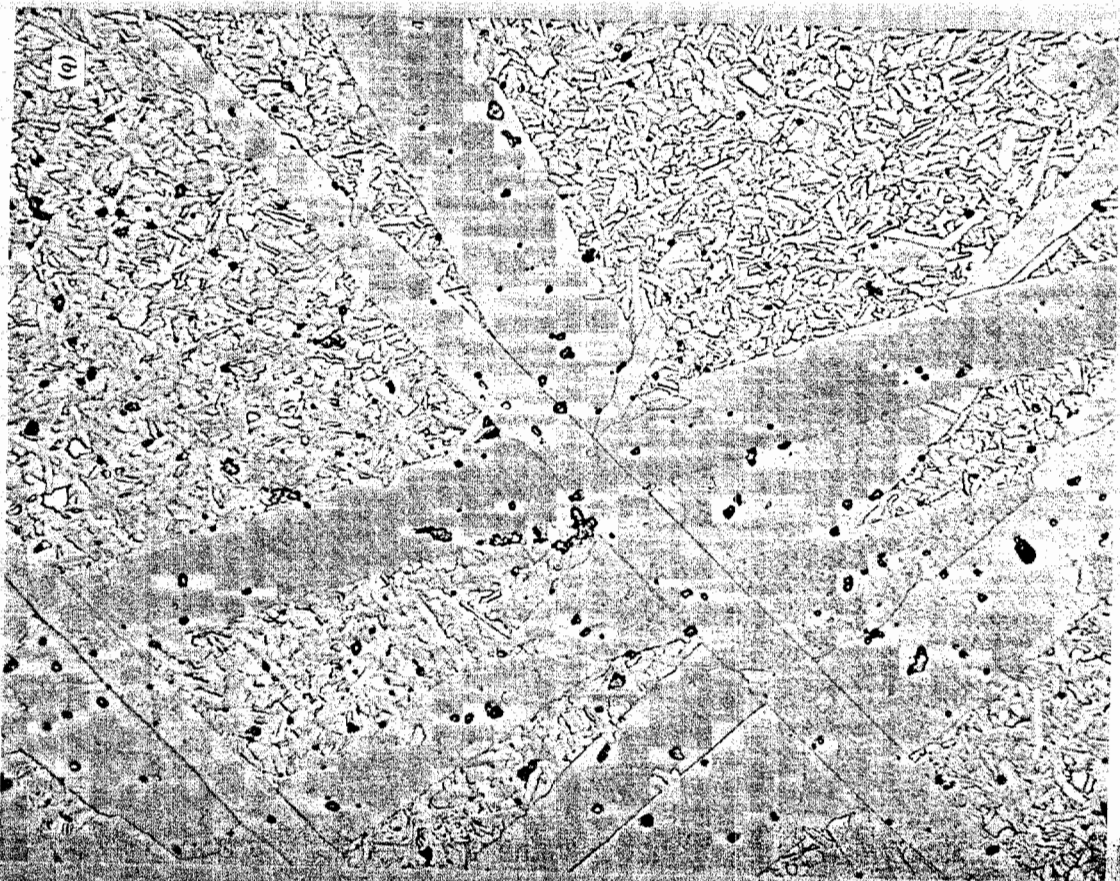


Fig. 10.15 (Continued). (b) Idiomorphic grains of  $\alpha$ -6H SiC in a  $\beta$ -SiC matrix (1000 $\times$ )

compact. Elimination of porosity is a related but separate subject and is considered in following sections. An application in which secondary recrystallization has been useful is in the development of preferred orientation on firing of the magnetically hard ferrite,  $\text{BaFe}_{12}\text{O}_{19}$ . \* For this

\*A. L. Stuifjes, *Trans. Brit. Ceram. Soc.*, 55, 57 (1956).

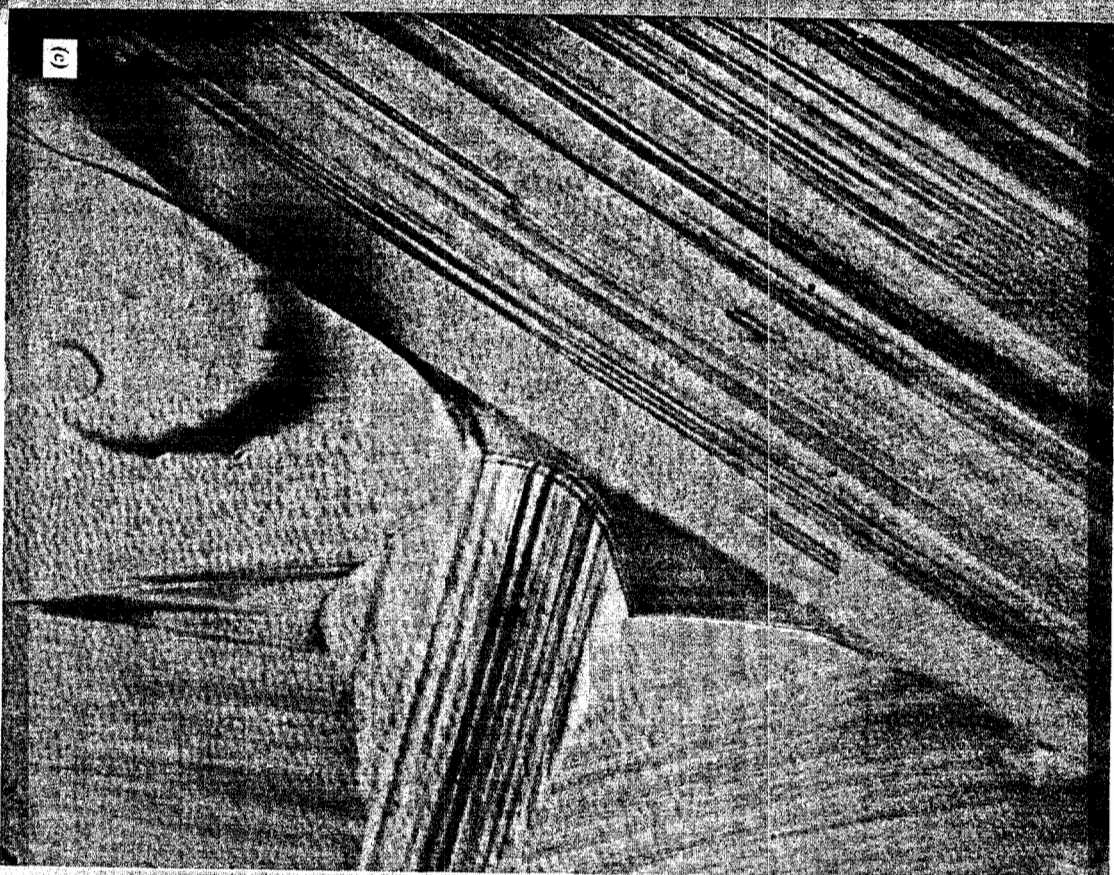


Fig. 10.15 (Continued). (c) Detail of boundary (75,000 $\times$ ). Courtesy S. Prochazka.

magnetic material it is desirable to obtain a high density as well as a high degree of preferred orientation in the sintered product. Particles of the powdered material can be oriented to a considerable extent by subjecting them to a high magnetic field while forming. On sintering there was a 57% alignment after heating at 1250°C. On further heating at 1340°C the

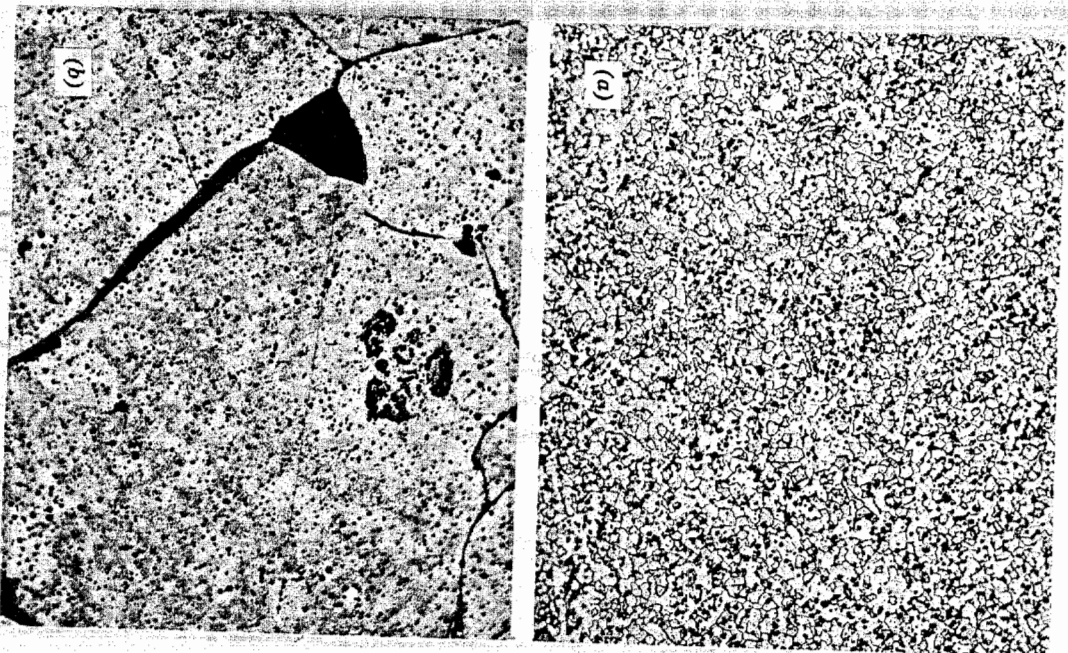


Fig. 10.16. A specimen of alumina (a) sintered 1 hr at 1800°C and (b) heated 1 hr at 1900°C to give secondary recrystallization. Note that the pore spacing has not changed. Courtesy of E. Burke.

preferred orientation increased to 93% alignment, corresponding to the structural change brought about by secondary recrystallization. It seems apparent that the few large grains in the starting material are more uniformly aligned than the fine surrounding material. These grains serve as nuclei for the secondary recrystallization process and give rise to a highly oriented final product.

## 10.2 Solid-State Sintering

Changes that occur during the firing process are related to (1) changes in grain size and shape, (2) changes in pore shape, and (3) changes in pore size. In Section 10.1 we concentrated on changes in grain size; in this and the following section we are mainly concerned with changes in porosity, that is, the changes taking place during the transformation of an originally porous compact to a strong, dense ceramic. As formed, a powder compact, before it has been fired, is composed of individual grains separated by between 25 and 60 vol% porosity, depending on the particular material used and the processing method. For maximizing properties such as strength, translucency, and thermal conductivity, it is desirable to eliminate as much of this porosity as possible. For some other applications it may be desirable to increase this strength without decreasing the gas permeability. These results are obtained during firing by the transfer of material from one part of the structure to the other. The kind of changes that may occur are illustrated in Fig. 10.17. The pores initially present can change shape, becoming channels or isolated spheres, without necessarily changing in size. More commonly, however, both the size and shape of the pores present change during the firing process, the pores becoming more spherical in shape and smaller in size as firing continues.

**Driving Force for Densification.** The free-energy change that gives rise to densification is the decrease in surface area and lowering of the surface free energy by the elimination of solid-vapor interfaces. This usually takes place with the coincidental formation of new but lower-energy

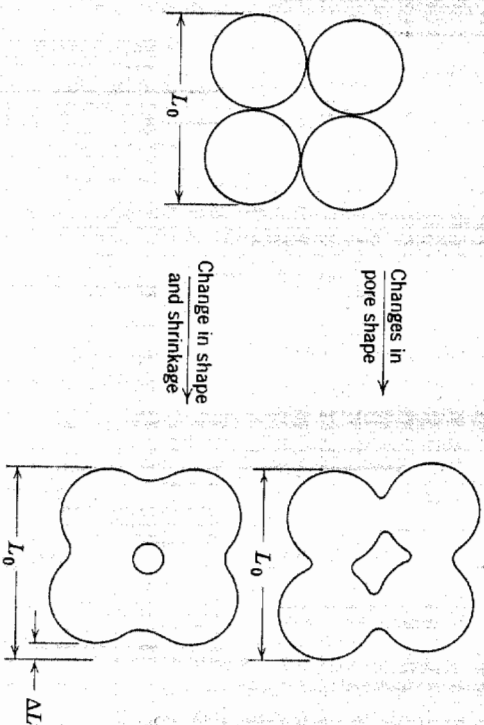


Fig. 10.17. Changes in pore shape do not necessarily require shrinkage.

solid-solid interfaces. The net decrease in free energy occurring on sintering a 1-micron particle size material corresponds to an energy decrease of about 1 cal/g. On a microscopic scale, material transfer is affected by the pressure difference and changes in free energy across a curved surface. These changes are due to the surface energy and have been discussed in Chapter 5 and referred to in Section 10.1. If the particle size, and consequently the radius of curvature, is small, these effects may be of a substantial magnitude. As indicated in Chapter 5, they become large when the radius of curvature is less than a few microns. This is one of the major reasons why much ceramic technology is based on and depends on the use of fine-particle materials.

Most of the insight into the effect of different variables on the sintering process has come from considering simple systems and comparing experimental data with simple models. Since our major aim is to be sure we understand the importance of different variables in traditional or new systems, we use this method here. Since the driving force is the same (surface energy) in all systems, considerable differences in behavior in various types of systems must be related to different mechanisms of material transfer. Several can be imagined—evaporation and condensation, viscous flow, surface diffusion, grain-boundary or lattice diffusion, and plastic deformation are among those that occur to us. Of these, diffusion and viscous flow are important in the largest number of systems; evaporation-condensation is perhaps the easiest to visualize.

**Evaporation-Condensation.** During the sintering process there is a tendency for material transfer because of the differences in surface curvature and consequently the differences in vapor pressure at various parts of the system. Material transfer brought about in this way is only important in a few systems; however, it is the simplest sintering process to treat quantitatively. We derive the sintering rate in some detail, since it provides a sound basis for understanding more complex processes.

Let us consider the initial stages of the process when the powder compact is just beginning to sinter and concentrate on the interaction between two adjacent particles (Fig. 10.18). At the surface of the particle there is a positive radius of curvature so that the vapor pressure is somewhat larger than would be observed for a flat surface. However, just at the junction between particles there is a neck with a small negative radius of curvature and a vapor pressure an order of magnitude lower than that for the particle itself. The vapor-pressure difference between the neck area and the particle surface tends to transfer material into the neck area.

We can calculate the rate at which the bonding area between particles increases by equating the rate of material transfer to the surface of the

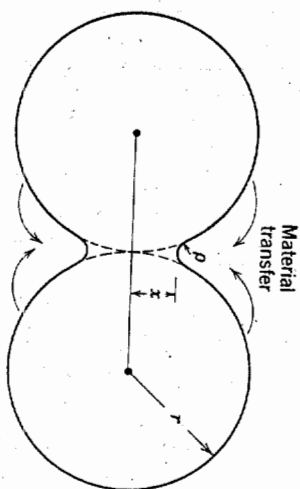


Fig. 10.18. Initial stages of sintering by evaporation-condensation.

lens between the spheres with the increase in its volume. The vapor pressure over the small negative radius of curvature is decreased because of the surface energy in accordance with the Thomson-Freundlich (Kelvin) equation discussed in Chapter 5:

$$\ln \frac{p_i}{p_0} = \frac{\gamma M}{dRT} \left( \frac{1}{\rho} + \frac{1}{x} \right) \quad (10.14)$$

where  $p_i$  is the vapor pressure over the small radius of curvature,  $M$  is the molecular weight of the vapor, and  $d$  is the density. In this case the neck radius is much larger than the radius of curvature at the surface,  $\rho$ , and the pressure difference  $p_0 - p_i$  is small. Consequently, to a good approximation,  $\ln p_i/p_0$  equals  $\Delta p/p_0$ , and we can write

$$\Delta p = \frac{\gamma M p_0}{d \rho RT} \quad (10.15)$$

where  $\Delta p$  is the difference between the vapor pressure of the small negative radius of curvature and the saturated vapor in equilibrium with the nearly flat particle surfaces. The rate of condensation is proportional to the difference in equilibrium and atmospheric vapor pressure and is given by the Langmuir equation to a good approximation as

$$m = \alpha \Delta p \left( \frac{M}{2\pi RT} \right)^{1/2} \quad \text{g/cm}^2/\text{sec} \quad (10.16)$$

where  $\alpha$  is an accommodation coefficient which is nearly unity. Then the rate of condensation should be equal to the volume increase. That is,

$$\frac{mA}{d} = \frac{dv}{dt} \quad \text{cm}^3/\text{sec} \quad (10.17)$$

From the geometry of the two spheres in contact, the radius of curvature at the contact points is approximately equal to  $x^2/2r$  for  $x/r$  less than 0.3;

the area of the surface of the lens between spheres is approximately equal to  $\pi^2 x^3/r$ ; the volume contained in the lenticular area is approximately  $\pi x^4/2r$ . That is,

$$\rho = \frac{x^2}{2r}; \quad A = \frac{\pi^2 x^3}{r}; \quad v = \frac{\pi x^4}{2r} \quad (10.18)$$

Substituting values for  $m$  in Eq. 10.16,  $A$  and  $v$  in Eq. 10.18 into Eq. 10.17 and integrating, we obtain a relationship for the rate of growth of the bond area between particles:

$$\frac{x}{r} = \left( \frac{3\sqrt{\pi}\gamma M^{3/2} p_0}{\sqrt{2} R^{3/2} T^{3/2} d^2} \right)^{1/3} r^{-2/3} t^{1/3} \quad (10.19)$$

This equation gives the relationship between the diameter of the contact area between particles and the variables influencing its rate of growth. The important factor from the point of view of strength and other material properties is the bond area in relation to the individual particle size, which gives the fraction of the projected particle area which is bonded together—the main factor in fixing strength, conductivity, and related properties. As seen from Eq. 10.19, the rate at which the area between particles forms varies as the two-thirds power of time. Plotted on a linear scale, this decreasing rate curve has led to characterizations of *end point* conditions corresponding to a certain sintering time. This concept of an end point is useful, since periods of time for sintering are not widely changed; however, the same rate law is observed for the entire process (Fig. 10.19b).

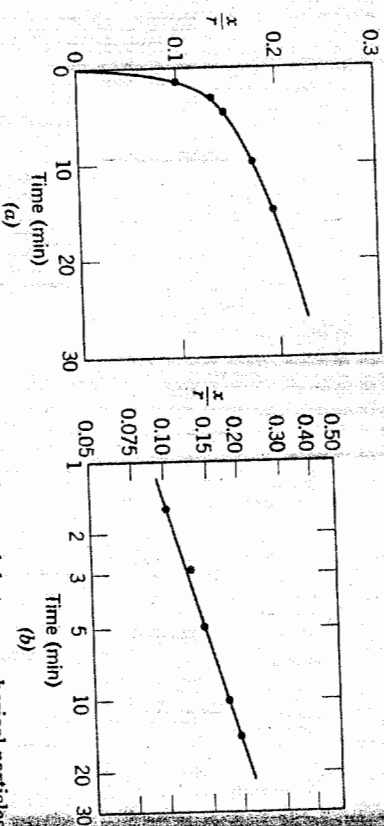


Fig. 10.19. (a) Linear and (b) log-log plots of neck growth between spherical particles of sodium chloride at 725°C.

If we consider the changes in structure that take place during a process such as this, it is clear that the distance between centers of spherical particles (Fig. 10.18) is not affected by the transfer of material from the particle surface to the interparticle neck. This means that the total shrinkage of a row of particles, or of a compact of particles, is unaffected by vapor-phase material transfer and that only the shape of pores is changed. This changing shape of pores can have an appreciable effect on properties but does not affect density.

The principal variables in addition to time that affect the rate of pore-shape change through this process are the initial particle radius (rate proportional to  $1/r^{2/3}$ ) and the vapor pressure (rate proportional to  $p_0^{1/3}$ ). Since the vapor pressure increases exponentially with temperature, the process of vapor-phase sintering is strongly temperature-dependent. From a processing point of view, the two main variables over which control can be exercised for any given material are the initial particle size and the temperature (which fixes the vapor pressure). Other variables are generally not easy to control, nor are they strongly dependent on conditions of use.

The negligible shrinkage corresponding to vapor-phase-material transfer is perhaps best illustrated in Fig. 10.20, which shows the shape changes that occur on heating a row of initially spherical sodium chloride particles. After long heating the interface contact area has increased; the

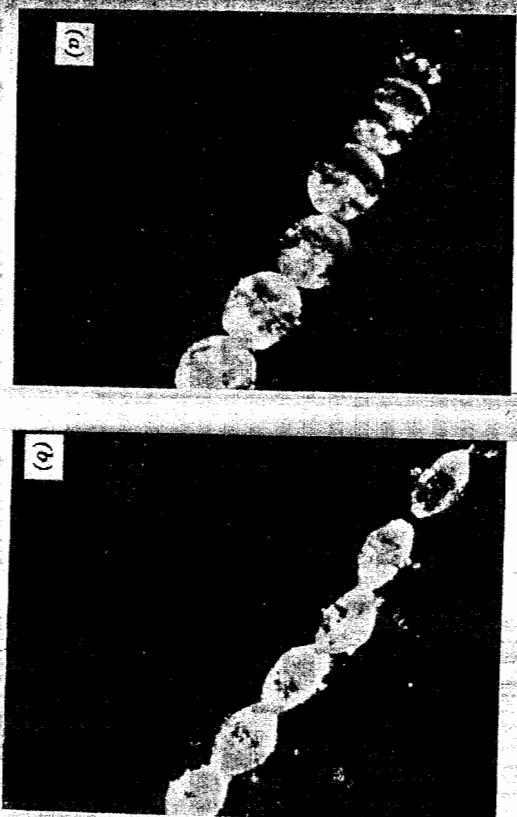


Fig. 10.20. Photomicrographs of sintering sodium chloride at 750°C: (a) 1 min; (b) 90 min.

particle diameter has been substantially decreased, but the distance between particle centers, that is, the shrinkage, has not been affected.

Vapor-phase material transfer requires that materials be heated to a temperature sufficiently high for the vapor pressure to be appreciable. For micron-range particle sizes this requires vapor pressures in the order of  $10^{-4}$  to  $10^{-5}$  atm, a pressure higher than those usually encountered during sintering of oxide and similar phases. Vapor-phase transfer plays an important part in the changes occurring during treatment of halides such as sodium chloride and is important for the changes in configuration observed in snow and ice technology.

**Solid-State Processes.** The difference in free energy or chemical potential between the neck area and the surface of the particle provides a driving force which causes the transfer of material by the fastest means available. If the vapor pressure is low, material transfer may occur more readily by solid-state processes, several of which can be imagined. As shown in Fig. 10.21 and Table 10.1, in addition to vapor transport (process 3), matter can move from the particle surface, from the particle bulk, or from the grain boundary between particles by surface, lattice, or grain-boundary diffusion. Which one or more of these processes actually contributes significantly to the sintering process in a particular system depends on their relative rates, since each is a parallel method of lowering the free energy of the system (parallel reaction paths have been discussed in Chapter 9). There is a most significant difference between these paths for matter transport: the transfer of material from the surface to the neck by surface or lattice diffusion, like vapor transport, does not lead to any decrease in the distance between particle centers. That is, these processes do not result in shrinkage of the compact and a decrease in porosity. Only

Table 10.1. Alternate Paths for Matter Transport During the Initial Stages of Sintering<sup>a</sup>

Mechanism Number	Transport Path	Source of Matter	Sink of Matter
1	Surface diffusion	Surface	Neck
2	Lattice diffusion	Surface	Neck
3	Vapor transport	Surface	Neck
4	Boundary diffusion	Grain boundary	Neck
5	Lattice diffusion	Grain boundary	Neck
6	Lattice diffusion	Dislocations	Neck

<sup>a</sup> See Fig. 10.21.

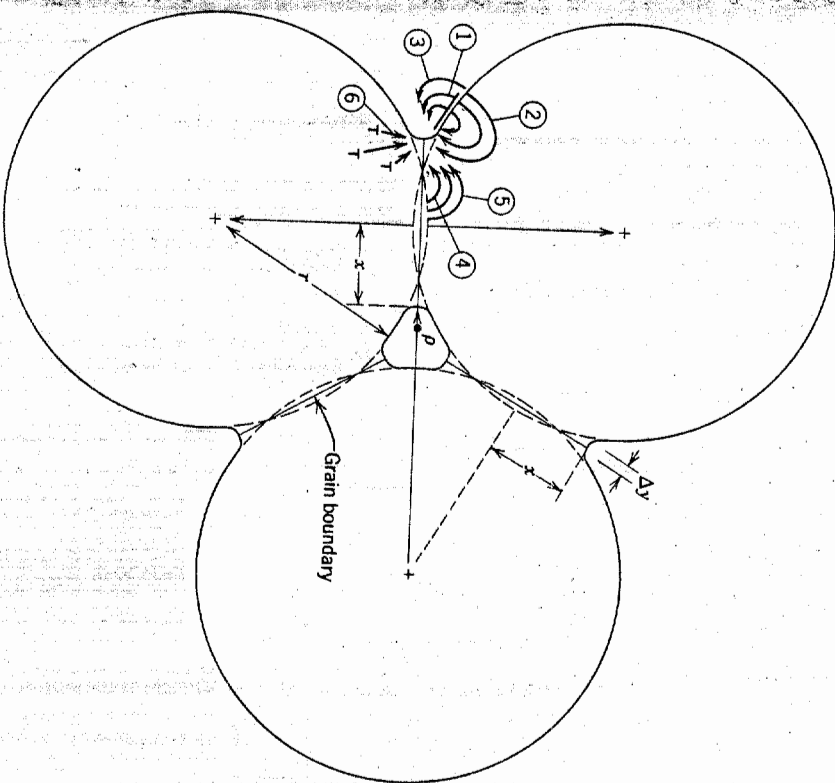


Fig. 10.21. Alternate paths for matter transport during the initial stages of sintering. Courtesy M. A. Ashby. (See Table 10.1.)

transfer of matter from the particle volume or from the grain boundary between particles causes shrinkage and pore elimination.

Let us consider mechanism 5, matter transport from the grain boundary to the neck by lattice diffusion. Calculation of the kinetics of this process is exactly analogous to determination of the rate of sintering by a vapor-phase process. The rate at which material is discharged at the surface area is equated to the increase in volume of material transferred. The geometry is slightly different:

$$\rho = \frac{x^2}{4r}, \quad A = \frac{\pi^2 x^3}{2r}, \quad V = \frac{\pi x^4}{4r} \quad (10.20)$$

The process can be visualized most easily by considering the rate of

migration of vacancies. In the same way that there are differences in vapor pressure between the surface of high negative curvature and the nearly flat surfaces, there is a difference in vacancy concentration. If  $c$  is the concentration of vacancies and  $\Delta c$  is the excess concentration over the concentration on a plane surface  $c_0$ , then, equivalent to Eq. 10.15,

$$\Delta c = \frac{\gamma a^3 c_0}{kT\rho} \quad (10.21)$$

where  $a^3$  is the atomic volume of the diffusing vacancy and  $k$  is the Boltzmann constant. The flux of vacancies diffusing away from the neck area per second per centimeter of circumferential length under this concentration gradient can be determined graphically and is given by

$$J = 4D_v \Delta c \quad (10.22)$$

Where  $D_v$  is the diffusion coefficient for vacancies,  $D_v$  equals  $D^*/a^3 c_0$  if  $D^*$  is the self-diffusion coefficient. Combining Eqs. 10.22 and 10.21 with the continuity equation similar to Eq. 10.17, we obtain the result

$$\frac{x}{r} = \left( \frac{40\gamma a^3 D^*}{kT} \right)^{1/5} r^{-3/5} t^{1/5} \quad (10.23)$$

With diffusion, in addition to the increase in contact area between particles, there is an approach of particles centers. The rate of this approach is given by  $d(x^2/2r)/dt$ . Substituting from Eq. 10.23, we obtain

$$\frac{\Delta V}{V_0} = \frac{3 \Delta L}{L_0} = 3 \left( \frac{20\gamma a^3 D^*}{\sqrt{2} kT} \right)^{2/5} r^{-6/5} t^{2/5} \quad (10.24)$$

These results indicate that the growth of bond formation between particles increases as a one-fifth power of time (a result which has been experimentally observed for a number of metal and ceramic systems) and that the shrinkage of a compact densified by this process should be proportional to the two-fifths power of time. The decrease in densification rate with time gives rise to an apparent end-point density if experiments are carried out for similar time periods. However, when plotted on a log-log basis, the change in properties is seen to occur as expected from Eq. 10.24. Experimental data for sodium fluoride and aluminum oxide are shown in Fig. 10.22.

The relationships derived in Eqs. 10.23 and 10.24 and similar relationships for the alternate matter transport processes, which we shall not derive, are important mainly for the insight that they provide on the variables which must be controlled in order to obtain reproducible processing and densification. It is seen that the sintering rate steadily decreases with time, so that merely sintering for longer periods to obtain

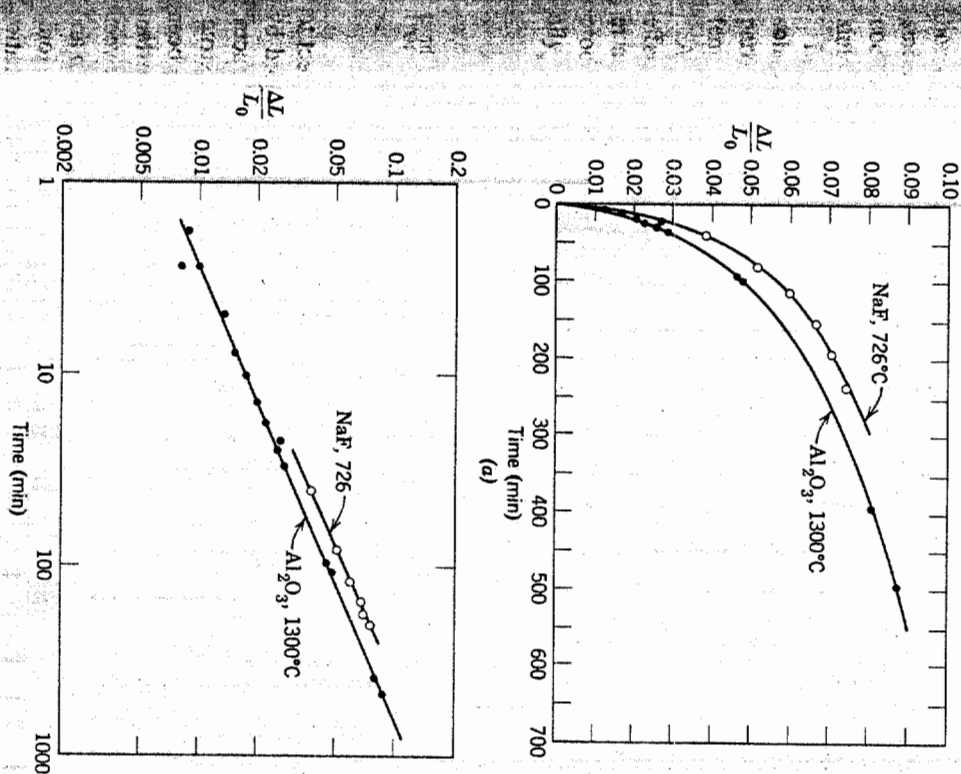


Fig. 10.22. (a) Linear and (b) log-log plots of shrinkage of sodium fluoride and aluminum oxide compacts. From J. E. Burke and R. L. Coble.

improved properties is impracticable. Therefore, time is not a major or critical variable for process control.

Control of particle size is very important, since the sintering rate is roughly proportional to the inverse of the particle size. The interface diameter achieved after sintering for a period of 100 hr at 1600°C is illustrated in Fig. 10.23 as a function of particle size. For large particles even these long periods do not cause extensive sintering; as the particle size is decreased, the rate of sintering is raised.

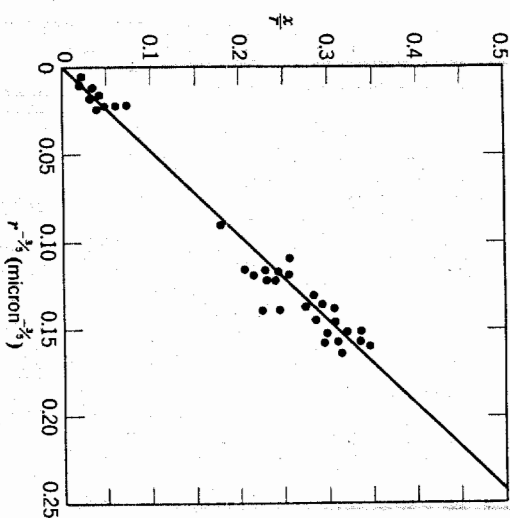


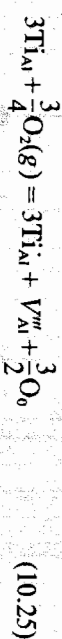
Fig. 10.23. Effect of particle size on the contact area growth in  $\text{Al}_2\text{O}_3$ , heated 100 hr at  $1600^\circ\text{C}$ . From R. L. Coble.

The other variable appearing in Eqs. 10.22 and 10.24 that is subject to analysis and some control is the diffusion coefficient; it is affected by composition and by temperature; the relative effectiveness of surfaces, boundaries, and volume as diffusion paths is affected by the microstructure. A number of relationships similar to Eqs. 10.23 and 10.24 have been derived, and it has been shown that surface diffusion is most important during early stages of sintering (these affect the neck diameter between particles but not the shrinkage or porosity); grain-boundary diffusion and volume diffusion subsequently become more important. In ionic ceramics, as discussed in Chapter 9, both the anion and the cation diffusion coefficients must be considered. In  $\text{Al}_2\text{O}_3$ , the best studied material, oxygen diffuses rapidly along the grain boundaries, and the more slowly moving aluminum ion at the boundary or in the bulk controls the overall sintering rate. As discussed in Chapter 5, the grain-boundary structure, composition, and electrostatic charge are influenced strongly by temperature and by impurity solutes; as discussed in Chapter 6, the exact mechanism of grain-boundary diffusion remains controversial. Estimates of the grain-boundary-diffusion width from sintering data range from 50 to 600 Å. These complications require us to be careful not to overanalyze data in terms of specific numerical results, since the time or temperature dependence of sintering may be in accordance with several plausible models. In general the presence of solutes which enhance either

boundary or volume diffusion coefficients enhance the rate of solid-state sintering. As discussed in Chapter 6, both boundary and volume diffusion coefficients are strongly temperature-dependent, which means that the sintering rate is strongly dependent on the temperature level.

In order to effectively control sintering processes which take place by solid-state processes, it is essential to maintain close control of the initial particle size and particle-size distribution of the material, the sintering temperature, the composition and frequently the sintering atmosphere.

As an example of the influence of solutes, Fig. 10.24 illustrates the effect of titania additions on the sintering rate of a relatively pure alumina in a region of volume diffusion. (Both volume and boundary diffusion processes are enhanced.) It is believed that Ti enters  $\text{Al}_2\text{O}_3$  substitutionally as  $\text{Ti}^{3+}$  and  $\text{Ti}^{4+}$  ( $\text{Ti}_{\text{Al}}$  and  $\text{Ti}_{\text{Al}}'$ ). At equilibrium



from which

$$K_1 = \frac{[\text{Ti}_{\text{Al}}]^3 [V_{\text{Al}}''']}{[\text{Ti}_{\text{Al}}]^3 [P_{\text{O}_2}]^{3/2}} \quad (10.26)$$

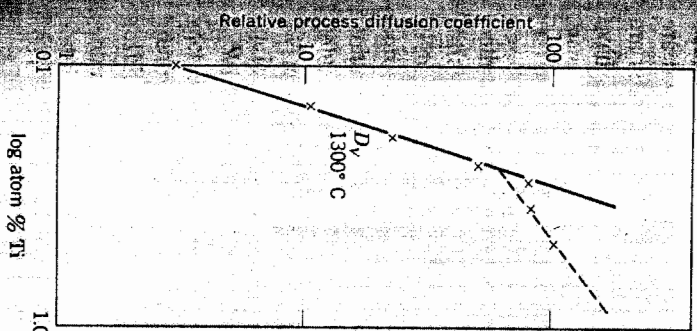


Fig. 10.24. Data for the relative sintering process diffusion coefficient with Ti additions to  $\text{Al}_2\text{O}_3$ .  $D_v[\text{Ti}]^3$ . From R. D. Bagley, I. B. Cutler, and D. L. Johnson, *J. Am. Ceram. Soc.*, 53, 136 (1970); R. J. Brook, *J. Am. Ceram. Soc.*, 55, 114 (1972).

In the powders used, divalent impurities such as magnesium exceed in concentrations the intrinsic defect levels, so that overall charge neutrality at moderate titania levels is achieved by

$$[\text{Ti}_i] = [\text{Mg}_{\text{Al}}] \quad (10.27)$$

and at constant impurity and oxygen pressure levels, combining Eqs. 10.26 and 10.27 gives

$$[V_{\text{Al}}''] = K_2 [\text{Ti}_{\text{Al}}]^3 \quad (10.28)$$

Since the total Ti addition ( $\text{Ti}_{\text{Al}} + \text{Ti}_{\text{Al}}'$ ) is much greater than the impurity levels,  $[\text{Ti}]_{\text{total}} \approx [\text{Ti}_{\text{Al}}]$  and  $[V_{\text{Al}}''] \approx K_2 [\text{Ti}]_{\text{total}}^3$ . The dependence of lattice defect concentrations on titania concentration is shown in Fig. 10.25 for the proposed model. As discussed in Chapter 6, the diffusion coefficient is proportional to the vacancy concentration; as a result the effect of this model is to anticipate an increase in the sintering rate proportional to the third power of titania concentration as experimentally observed (Fig. 10.24). At higher concentrations the dependence on titania concentration should become less steep, which is suggested by the sintering data.

Thus far our discussion of the variables influencing the sintering process has been based on the initial stages of the process, in which models are based on solid particles in contact. As the process continues, an intermediate microstructure forms in which the pores and solid are both continuous, followed by a later stage in which isolated pores are separated from one another. A number of analytical expressions have

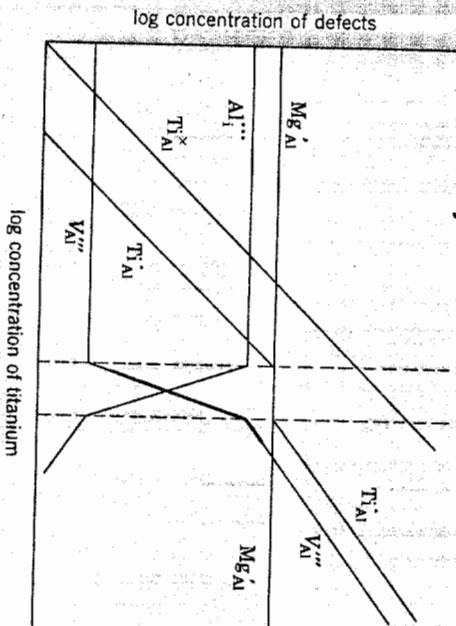


Fig. 10.25. Model for the dependence of defect concentrations on the Ti concentration in  $\text{Al}_2\text{O}_3$ . From R. J. Brook, *J. Am. Ceram. Soc.*, 55, 114 (1972).

been derived from specific microstructural models for the transport processes listed in Table 10.1. In the later stages of the process only two mechanisms are important: boundary diffusion from sources on the boundary and lattice diffusion from sources on the boundary. For a nearly spherical pore the flux of material to a pore can be approximated as

$$J = 4\pi D_v \Delta c \left( \frac{rR}{R-r} \right) \quad (10.29)$$

where  $D_v$  is the volume diffusion coefficient,  $\Delta c$  is the excess vacancy concentration (Eq. 10.21),  $r$  is the pore radius, and  $R$  is the effective material-source radius. The importance of microstructure in applying this sort of analysis to specific systems is illustrated in Fig. 10.26. For a sample

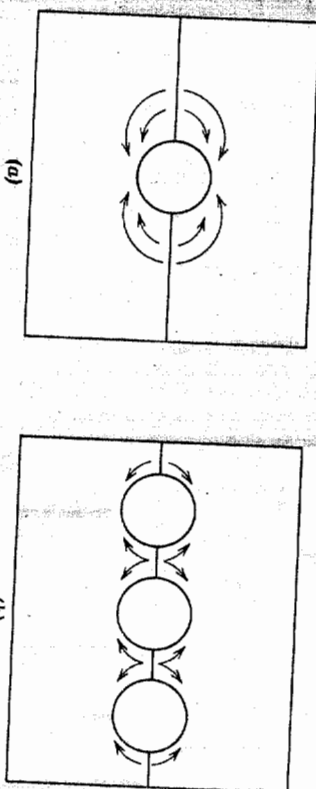


Fig. 10.26. The mean diffusion distance for material transport is smaller when there are more of the same size of pores in a boundary.

with a larger number of pores, all the same size, on a boundary the mean diffusion distance is smaller when there are more pores, and pore elimination is accomplished more quickly for the sample with the higher porosity. Thus, although the terms which influence the rate of sintering—volume or boundary diffusion coefficient (and therefore temperature and solute concentration) surface energy and pore size—are well established, the geometrical relationship of grain boundaries to the pores may have a variety of forms and is critical in determining what actually occurs.

With fine-grained materials such as oxides, it is usual to observe an increase in both grain size and pore size during the early stages of heat treatment, as illustrated for Lucalox alumina in Fig. 10.27. This partially results from the presence of agglomerates of the fine particles which sinter rapidly, leaving interagglomerate pores, and is partly due to the rapid grain growth during which pores are agglomerated by moving with the boundaries, as illustrated in Fig. 10.9. In cases in which agglomeration

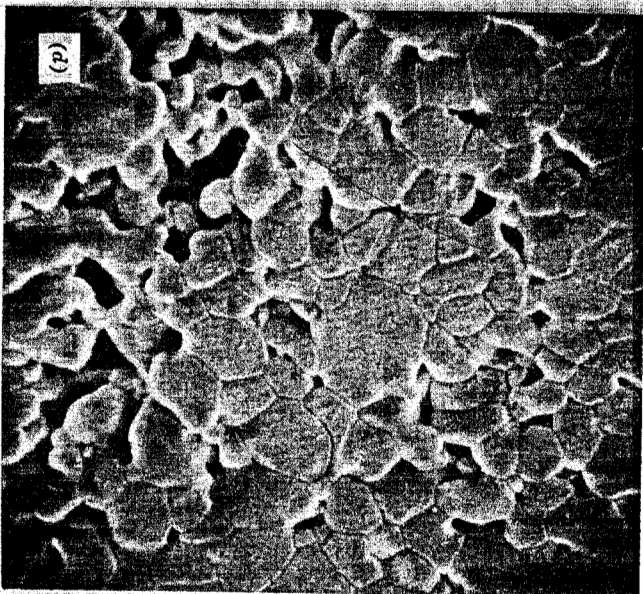
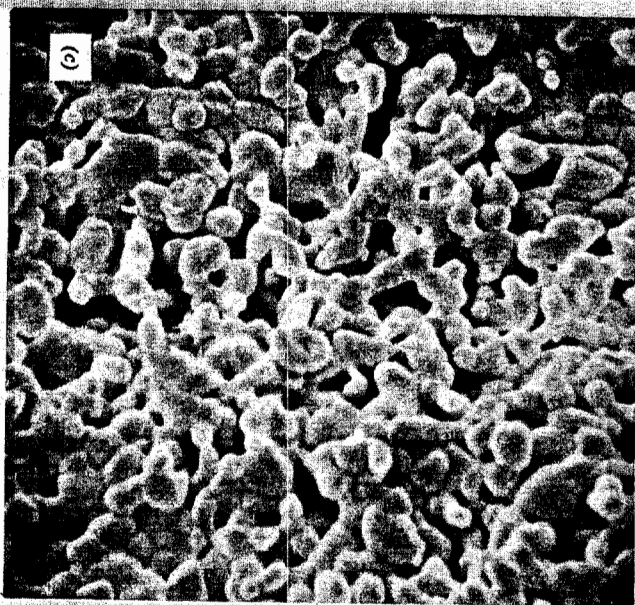
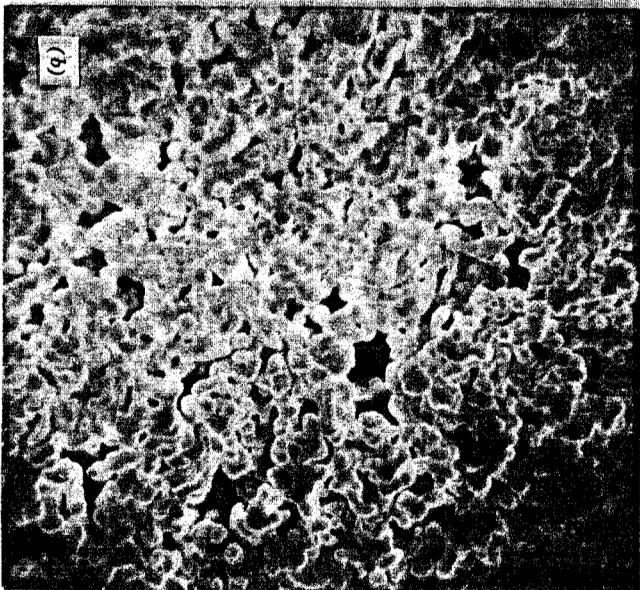


Fig. 10.27. Progressive development of microstructure in Lucalox alumina. Scanning electron micrographs of (a) initial particles in the compact (5000 $\times$ ), (b) after 1 min at 1700°C (5000 $\times$ ).

Fig. 10.27 (Continued) (c) Scanning electron micrographs after 2 1/2 min at 1700°C (5000 $\times$ ), and (d) after 6 min at 1700°C (5000 $\times$ ). Note that pores and grains increase in size, that there are variations in packing and in pore size, and that pores remain located between dense grains.

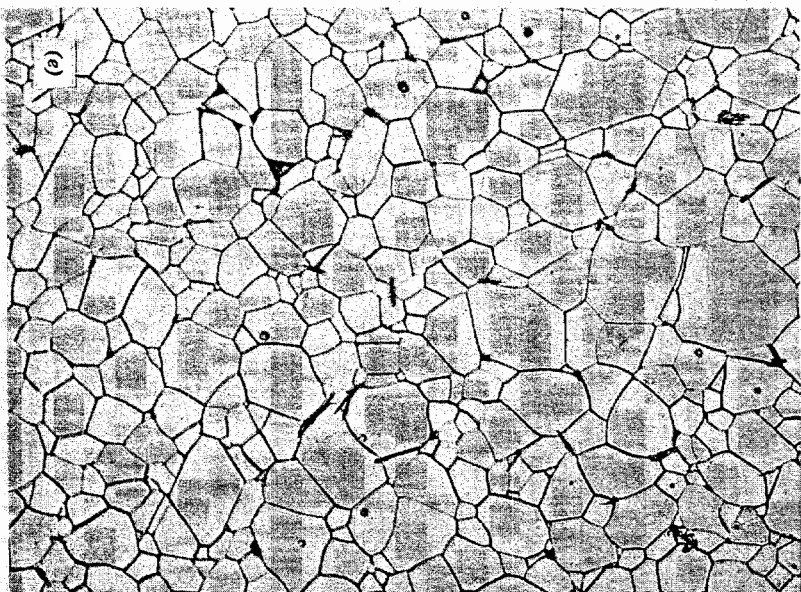


Fig. 10.27 (Continued) (e) The final microstructure is nearly porefree, with only a few pores located within grains (500 $\times$ ). Courtesy C. Greskovich and K. W. Lay.

of fine precipitated particles into clumps is severe, ball milling to break up the agglomerates leads to a remarkable increase in the sintering rate. Even minor variations in the original particle packing are exaggerated during the pore growth process; in addition, spaces between agglomerates and occasional larger voids resulting from the bridging of particles or agglomerates are present. As a result, during intermediate stages of the sintering process there is a range of pore sizes present, and the slower elimination of the larger pores leads to variations in pore concentration in the later stages of the sintering process, as illustrated in Fig. 10.28c.

In addition to local agglomerates and packing differences, pore concentration variations in the later stages of sintering can result from particle-size variations in the starting material, from green density variations

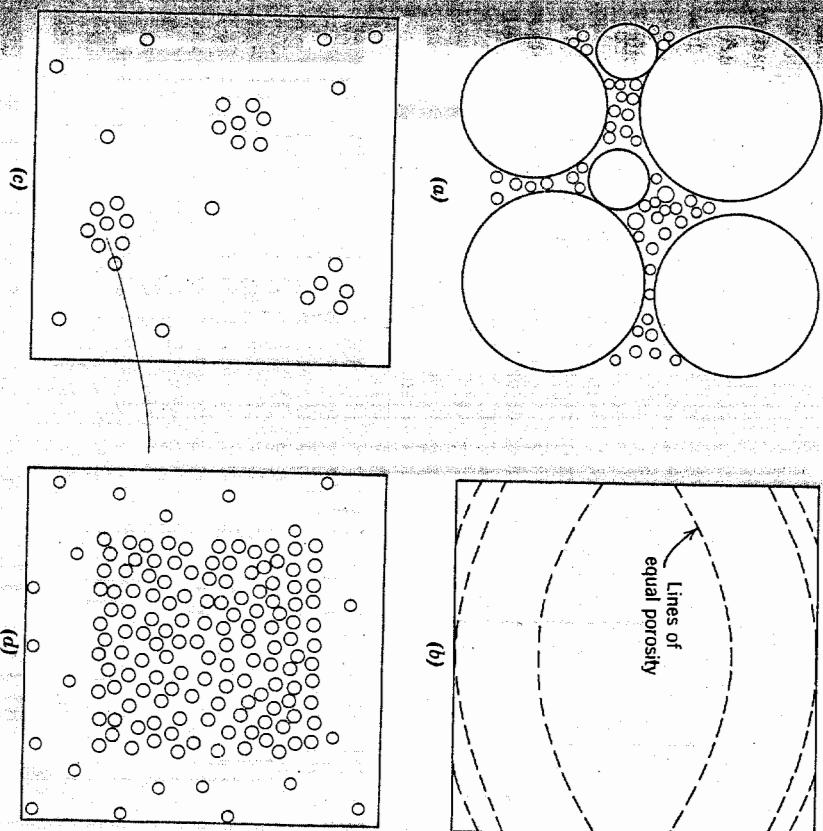


Fig. 10.28. Pore-concentration variations resulting from (a) a variation in grain sizes, (b) die friction, (c) local packing and agglomeration differences, and (d) more rapid pore elimination near surfaces.

tions caused by die-wall friction during pressing, and from the more rapid elimination of porosity near surfaces caused by temperature gradients during heating, as shown in Fig. 10.28. The importance of local variations in pore concentration results from the fact that the part of the sample containing pores tends to shrink but is restrained by other pore-free parts. That is, the effective diffusion distance is no longer from the pore to an adjacent grain boundary but a pore-pore or pore-surface distance many orders of magnitude larger. An example of residual pore clusters in a sintered oxide is shown in Fig. 10.29.

Not only the kinetics of pore elimination can lead to "stable" and residual porosity, but it is also possible in some cases to have a thermodynamically metastable equilibrium pore configuration. In Fig.

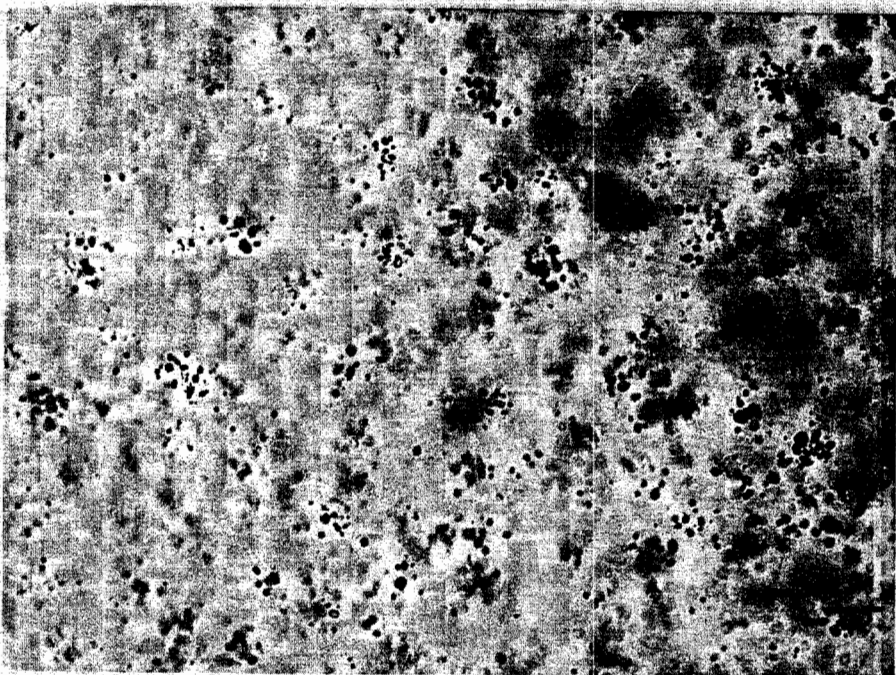


Fig. 10.29. Residual pore clusters resulting from improper powder processing in a sample of 90 mole %  $\text{Y}_2\text{O}_3$ -10 mole %  $\text{ThO}_2$ . Transmitted light, 137 $\times$ . Courtesy C. Greskovich and K. N. Woods.

10.26 we have drawn spherical pores located on a grain boundary, the usual model description, but we know from our discussion of interface energies in Chapter 5 that there is a dihedral angle  $\phi$  at the pore-boundary intersection determined by the relative interface energies;

$$\cos \frac{\phi}{2} = \frac{\gamma_{sp}}{2\gamma_s} \quad (10.30)$$

In most cases the dihedral angle for pure oxides is about  $150^\circ$ , and the spherical pore approximation is quite good; but for  $\text{Al}_2\text{O}_3 + 0.1\% \text{MgO}$  the

value is  $130^\circ$ , for  $\text{UO}_2 + 30 \text{ ppm C}$  the value is  $88^\circ$ , and for impure boron carbide the value is about  $60^\circ$ . For these materials the consequences of nonspherical pores have to be considered.

As discussed for discontinuous grain growth and illustrated in Figs. 10.4 and 10.11, the boundary curvature between grains or phases depends both on the value of the dihedral angle and on the number of surrounding grains. If we take  $r$  as the radius of a circumscribed sphere around a polyhedral pore surrounded by grains, the ratio of the radius of curvature of the pore surfaces  $\rho$  to the spherical radius depends both on the dihedral angle and on the number of surrounding grains, as shown in Fig. 10.30a. When  $r/\rho$  decreases to zero, the interfaces are flat and have no tendency

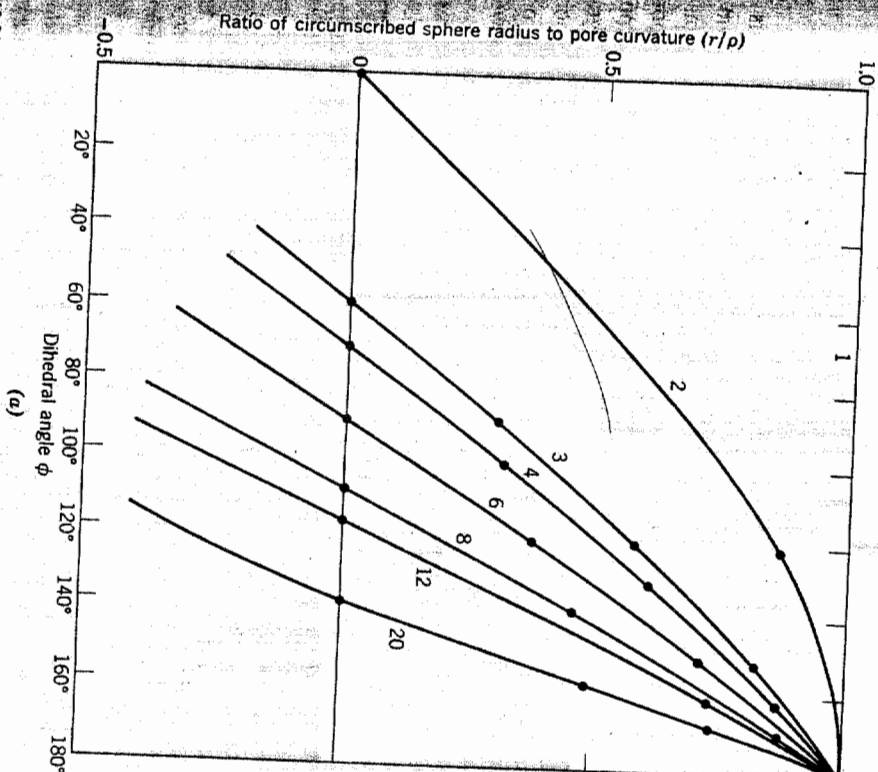


Fig. 10.30. (a) Change in the ratio ( $r/\rho$ ) with dihedral angle for pores surrounded by different numbers of grains as indicated on individual curves.

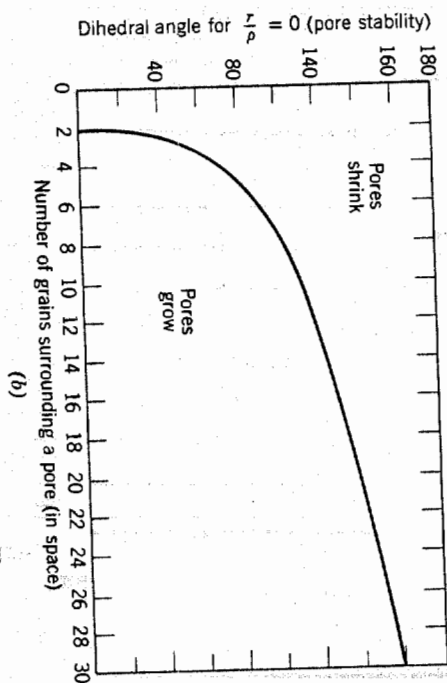


Fig. 10.30 (Continued). (b) Conditions for pore stability.

for shrinkage; when  $r/\rho$  is negative, the pore tends to grow. This is illustrated in Fig. 10.30b. For a uniform grain size the space-filling form is a tetrakaidecahedron with 14 surrounding grains. From an approximate relationship between the number of surrounding grains and the pore diameter to grain-diameter ratio we can derive a relationship for pore stability as a function of dihedral angle and the ratio of pore size to grain size, as shown in Fig. 10.31. From this figure we can see why large pores present in poorly compacted powder such as shown in Fig. 10.32 not only remain stable but grow. It is also seen that an enormous disparity between

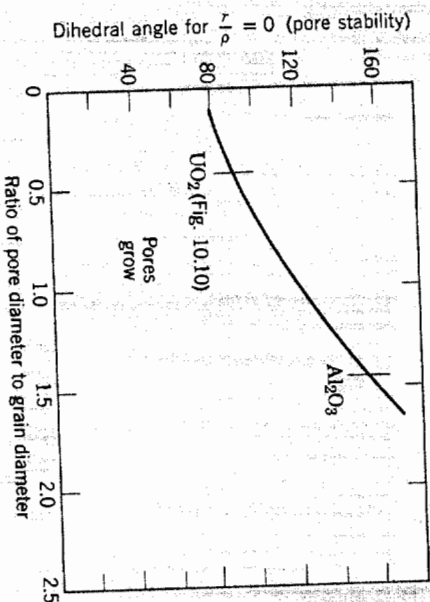


Fig. 10.31. Conditions for pore stability.

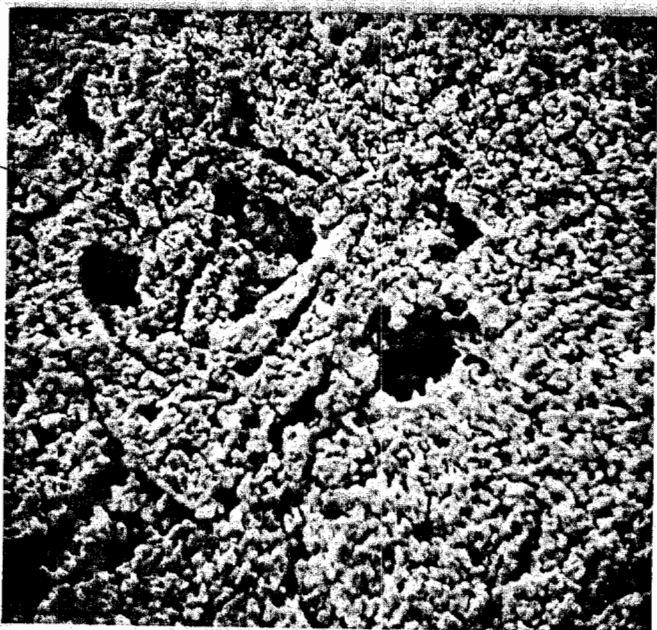


Fig. 10.32. Large voids formed by bridging of agglomerates in fine  $\text{Al}_2\text{O}_3$  powder viewed with scanning electron microscope at 2000 $\times$ . Courtesy C. Greskovich.

grain size and pore size is not necessary for pore stability. That is, the site and size of the porosity relative to the grain-boundary network not only affects the necessary distance for diffusion but also the driving force for the process.

The interaction of grain boundaries and porosity is, of course, a two-way street. When many pores are present during the initial stages of sintering, grain growth is inhibited. However, as discussed in Section 10.1, once the porosity has decreased to a value such that secondary grain growth can occur, extensive grain growth may result at high sintering temperatures. When grain growth occurs, many pores become isolated from grain boundaries, and the diffusion distance between pores and a grain boundary becomes large, and the rate of sintering decreases. This is illustrated in Fig. 10.16b, in which extensive secondary recrystallization has occurred, with the isolation of pores in the interior of grains and a reduction in the densification rate. Similarly, the sample of aluminum oxide shown in Fig. 10.33 has been sintered at a high temperature at which discontinuous grain growth occurred. Porosity is only removed near the grain boundaries, which act as the vacancy sink. The importance of

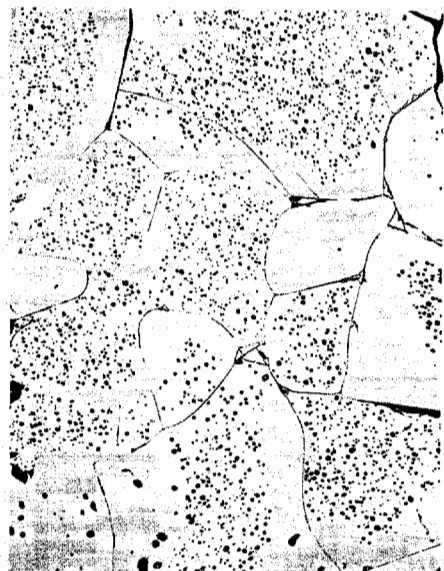


Fig. 10.33. Sintered  $\text{Al}_2\text{O}_3$  illustrating elimination of porosity adjacent to grain boundaries with residual porosity remaining at grain centers. Courtesy J. E. Burke.

controlling grain growth as an integral part of controlling sintering phenomena cannot be overestimated. Consequently, the grain-growth processes discussed in Section 10.1 must be actively prevented in order to obtain complete densification. Usually densification continues by a diffusion process until about 10% porosity is reached; at this point rapid grain growth occurs by secondary recrystallization, and the rate of densification is sharply reduced. In order to obtain densification much beyond this level, prevention of secondary recrystallization is essential. The most satisfactory way of doing this is with additives which prevent or slow down boundary migration to a point at which it is possible to obtain pore elimination. Additions of  $\text{MgO}$  to  $\text{Al}_2\text{O}_3$ ,  $\text{ThO}_2$  to  $\text{Y}_2\text{O}_3$ , and  $\text{CaO}$  to  $\text{ThO}_2$  among others, have been found to slow boundary migration and allow complete pore elimination by solid-state sintering in these systems. The porefree microstructure of a polycrystalline ceramic having optical transparency suitable for use as a laser material is shown in Fig. 10.34.

### 10.3 Vitrification

To vitrify is to make glasslike and the vitrification process—densification with the aid of a viscous liquid phase—is the major firing process for the great majority of silicate systems. (In some current glossaries vitrification is defined as being identical to densification on firing, but the more specific usage is preferred.) A viscous liquid silicate is formed at the firing temperature and serves as a bond for the body. For

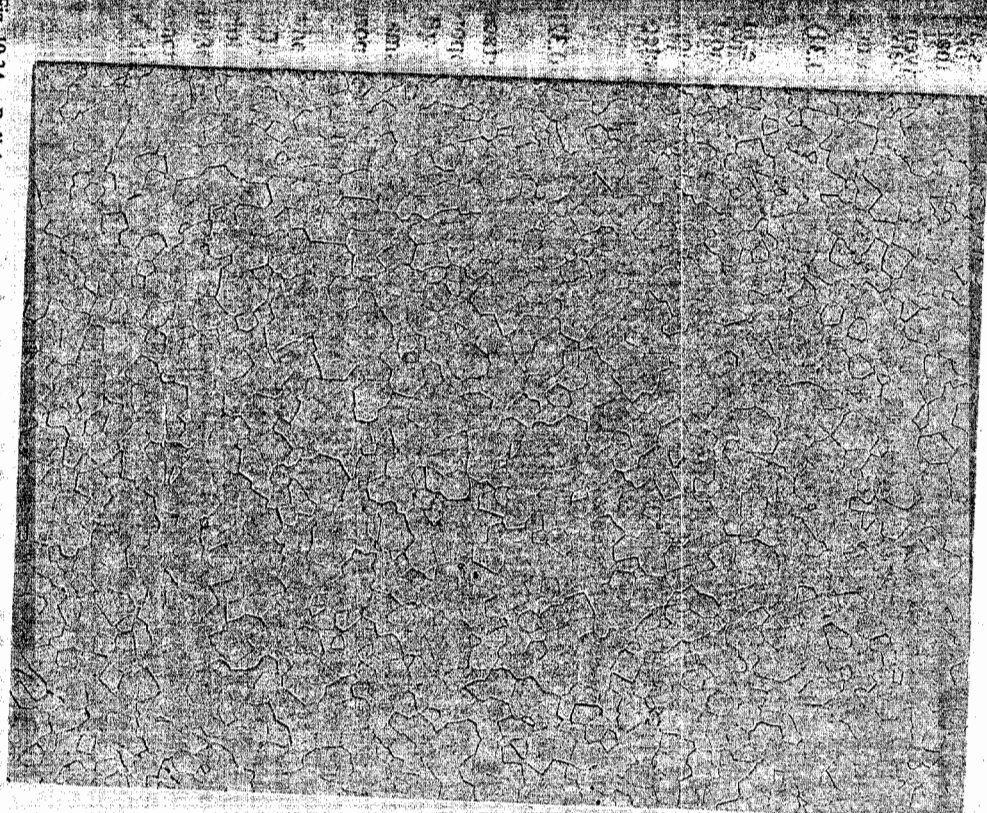


Fig. 10.34. Polished section of  $\text{Y}_2\text{O}_3 + 10$  mole %  $\text{ThO}_2$  sintered to porefree state. 100 $\times$ . Courtesy C. Greskovich and K. N. Woods.

satisfactory firing the amount and viscosity of the liquid phase must be such that densification occurs in a reasonable time without the ware slumping or warping under the force of gravity. The relative and absolute rates of these two processes (shrinkage and deformation) determine to a large extent the temperature and compositions suitable for satisfactory firing.

**Process Kinetics.** If we consider two particles initially in contact (Fig. 10.21), there is a negative pressure at the small negative radius of

curvature  $\rho$  compared with the surface of the particles. This causes a viscous flow of material into the pore region. By an analysis similar to that derived for the diffusion process, the rate of initial neck growth is given as\*

$$\frac{x}{r} = \left( \frac{3\gamma}{2\eta\rho} \right)^{1/2} t^{1/2} \quad (10.31)$$

The increase in contact diameter is proportional to  $t^{1/2}$ ; the increase in area between particles is directly proportional to time. Factors of most importance in determining the rate of this process are the surface tension, viscosity, and particle size. The shrinkage which takes place is determined by the approach between particle centers and is

$$\frac{\Delta V}{V_0} = \frac{3}{L_0} \frac{\Delta L}{L_0} = \frac{9\gamma}{4\eta r} t \quad (10.32)$$

That is, the initial rate of shrinkage is directly proportional to the surface tension, inversely proportional to the viscosity, and inversely proportional to the particle size.

The situation after long periods of time can best be represented as small spherical pores in a large body (Fig. 10.35). At the interior of each pore

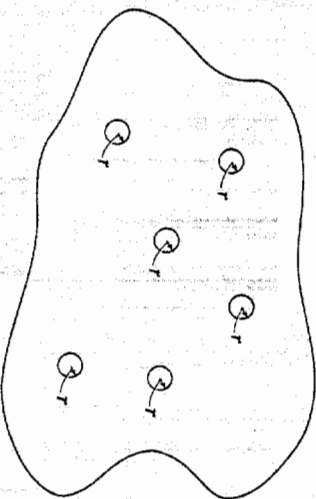


Fig. 10.35. Compact with isolated spherical pores near the end of the sintering process.

there is a negative pressure equal to  $2\gamma/r$ ; this is equivalent to an equal positive pressure on the exterior of the compact tending to consolidate it. J. K. Mackenzie and R. Shuttleworth† have derived a relation for the rate of shrinkage resulting from the presence of isolated equal-size pores in a viscous body. The effect of surface tension is equivalent to a pressure of  $-2\gamma/r$  inside all pores or, for an incompressible material, to the applica-

tion of a hydrostatic pressure of  $+2\gamma/r$  to the compact. The real problem is to deduce the properties of the porous material from the porosity and viscosity of the dense material. The method of approximation used gives an equation of the form

$$\frac{d\rho'}{dt} = \frac{2}{3} \left( \frac{4\pi}{3} \right)^{1/3} n^{1/3} \frac{\gamma}{\eta} (1 - \rho')^{2/3} \rho'^{1/3} \quad (10.33)$$

where  $\rho'$  is the relative density (the bulk density divided by the true density or the fraction of true density which has been reached) and  $n$  is the number of pores per unit volume of real material. The number of pores depends on the pore size and relative density and is given by

$$\frac{4\pi}{3} r^3 = \frac{\text{Pore volume}}{\text{Solid volume}} = \frac{1 - \rho'}{\rho'} \quad (10.34)$$

$$n^{1/3} = \left( \frac{1 - \rho'}{\rho'} \right)^{1/3} \left( \frac{3}{4\pi} \right)^{1/3} \frac{1}{r} \quad (10.35)$$

By combining with Eq. 10.33,

$$\frac{d\rho'}{dt} = \frac{3\gamma}{2r_0\eta} (1 - \rho') \quad (10.36)$$

where  $r_0$  is the initial radius of the particles.

The general course of the densification process is best represented by a plot of relative density versus nondimensional time, illustrated in Fig. 10.36 following Eq. 10.33. Spherical pores are formed very quickly to reach a relative density of about 0.6. From this point until the completion of the sintering process about one unit of nondimensional time is

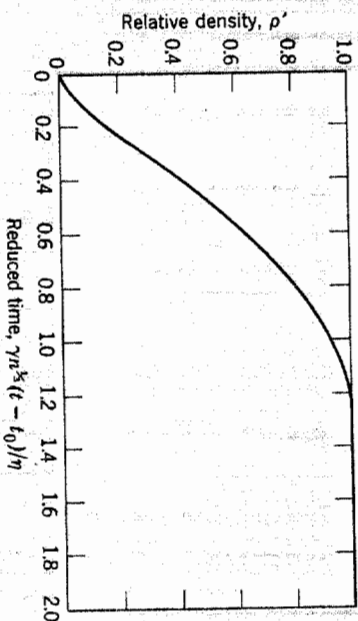


Fig. 10.36. Increase in relative density of compact with reduced time for a viscous material. From J. K. Mackenzie and R. Shuttleworth, *Proc. Phys. Soc. (London)*, B62, 833 (1949).

\*J. Frenkel, *J. Phys. (USSR)*, 9, 385 (1945).

†*Proc. Phys. Soc. (London)*, B62, 833 (1949).

required. For complete densification

$$t_{\text{rec}} \sim \frac{1.5r_0\eta}{\gamma} \quad (10.37)$$

Some experimental data for the densification of a viscous body are shown in Fig. 10.37, in which the strong effect of temperature, that is, the viscosity of the material, is illustrated by the rapid change in sintering rates. The solid lines in Fig. 10.37 are calculated from Eq. 10.33. The

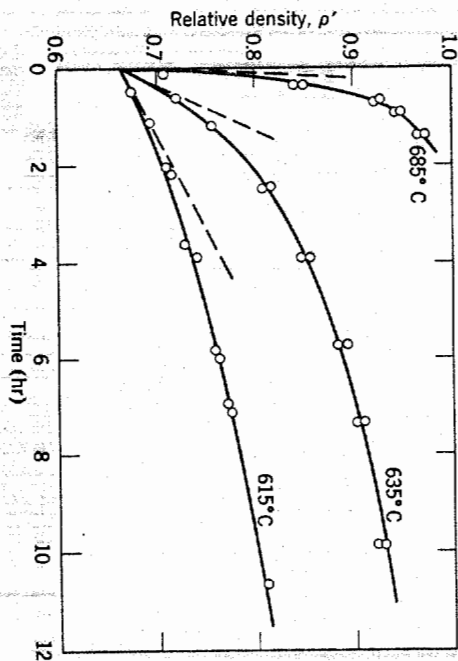


Fig. 10.37. Densification of a soda-lime-silica glass.

initial rates of sintering indicated by the dashed curves are calculated from Eq. 10.32. The good agreement of these relationships with the experimental results gives us confidence in applying them to vitrification processes in general.

**Important Variables.** The particular importance of Eqs. 10.31 to 10.37 is the dependence of the rate of densification on three major variables—the particle size, viscosity, and surface tension. For silicate materials the surface tension is not changed much by composition, although there are some systems for which surface energy is particularly low, as illustrated in Chapter 5. However, surface tension is not a variable that normally causes difficulty during the design of compositions or the control of processing. The particle size has a strong effect on the sintering rate and must be closely controlled if the densification process is going to be controlled. In changing from a 10-micron to 1-micron particle, the rate of sintering is increased by a factor of 10. Even more important for control

purposes is the viscosity and its rapid change with temperature. For a typical soda-lime-silica glass the viscosity changes by a factor of 1000 over an interval of 100°C; the rate of densification changes by an equal factor over the temperature range. This means that the temperature must be closely controlled. Viscosity is also much changed by composition, as discussed in Chapter 3. The rate of densification, then, can be increased by changing the composition to lower the viscosity of the glassy material. The relative values of viscosity and particle size are also important; the viscosity must not be so low that appreciable deformation takes place under the forces of gravity during the time required for densification. This makes it necessary for the particle size to be in such a range that the stresses due to surface tension are substantially larger than the stresses due to gravitational forces. Materials sintered in a fluid state must be supported so that deformation does not occur. The best means of obtaining densification without excessive deformation is to use very fine-grained materials and uniform distribution of materials. This requirement is one of the reasons why successful compositions in silicate systems are composed of substantial parts of talc and clays that are naturally fine-grained and provide a sufficient driving force for the vitrification process.

**Silicate Systems.** The importance of the vitrification process lies in the fact that most silicate systems form a viscous glass at the firing temperature and that a major part of densification results from viscous flow under the pressure caused by fine pores. Questions that naturally arise are how much liquid is present and what are its properties. Let us consider Fig. 7.26, which shows an isothermal cut at 1200°C in the  $K_2O-Al_2O_3-SiO_2$  system; this is the lower range of firing temperatures used for semivitreous porcelain bodies composed of about 50% kaolin (45%  $Al_2O_3$ , 55%  $SiO_2$ ), 25% potash-feldspar, and 25% silica. This and similar compositions are in the primary field of mullite, and at 1200°C there is an equilibrium between mullite crystals and a liquid having a composition approximately 75%  $SiO_2$ , 12.5%  $K_2O$ , 12.5%  $Al_2O_3$ , not much different in composition from the eutectic liquid in the feldspar-silica system (Fig. 7.14). In actual practice only a small part of the silica present as flint enters into the liquid phase, and the composition of the liquid depends on the fineness of the grinding as well as on the overall chemical composition. However, the amount of silica which dissolves does not have a large effect on the amount and composition of the liquid phase present. The liquid is siliceous and has a high viscosity; the major effect of compositional changes is to alter the relative amounts of mullite and liquid phases present. Since mullite is very fine-grained, the fluid flow properties of the body correspond to those of a liquid having a viscosity greater than the pure liquid phase. For

some systems the overall flow process corresponds to plastic flow with a yield point rather than to true viscous flow. This changes the kinetics of the vitrification process by introducing an additional term in Eqs. 10.33 and 10.36 but does not change the relative effects of different variables.

Although phase diagrams are useful, they do not show all the effects of small changes in composition. For example, a kaolinite composition should show equilibrium between mullite and tridymite at 1400°C with no glassy material. However, it is observed experimentally that even after 24 hr about 60 vol% of the original starting material is amorphous and deforms as a liquid. The addition of a small amount of lithium oxide as  $\text{Li}_2\text{CO}_3$  has been observed to give a larger content of glass than additions of the same composition as the fluoride. Similar small amounts of other mineralizers can also have a profound effect in the firing properties of particular compositions. That fine grinding and intimate mixing reduce the vitrification temperature follows from the analysis in Eqs. 10.31 to 10.37. S. C. Sane and R. L. Cook\* found that ball milling for 100 hr reduced the final porosity of a clay-feldspar-flint composition from 17.1 to 0.3% with the same firing conditions. This change is caused in part by increased tendencies toward fusion equilibrium and uniform mixing of constituents and in part by the smaller initial particle and pore size. In contrast to triaxial (flint-feldspar-clay) porcelain, which frequently do not reach fusion equilibrium, many steatite bodies and similar compositions which are prepared with fine-particle, intimately mixed material and form a less siliceous liquid reach phase equilibrium early in the firing process.

The time-temperature relationship and the great dependence of vitrification processes on temperature can perhaps be seen best in the experimental measurements illustrated in Fig. 10.38. As shown there, the time required for a porcelain body to reach an equivalent maturity changes by almost an order of magnitude with a 50° temperature change. There are changes in both the amount and viscosity of the glassy phase during firing, so that it is difficult to elucidate a specific activation energy for the process with which to compare the activation energy for viscous flow. However, the temperature dependence of the vitrification rate of a composition such as this (a mixture of clay, feldspar, and flint) is greater than the temperature dependence of viscosity alone. This is to be expected from the increased liquid content at the higher firing temperatures.

In summary, the factors determining the vitrification rate are the pore size, viscosity of the overall composition (which depends on amount of liquid phase present and its viscosity), and the surface tension. Equivalent

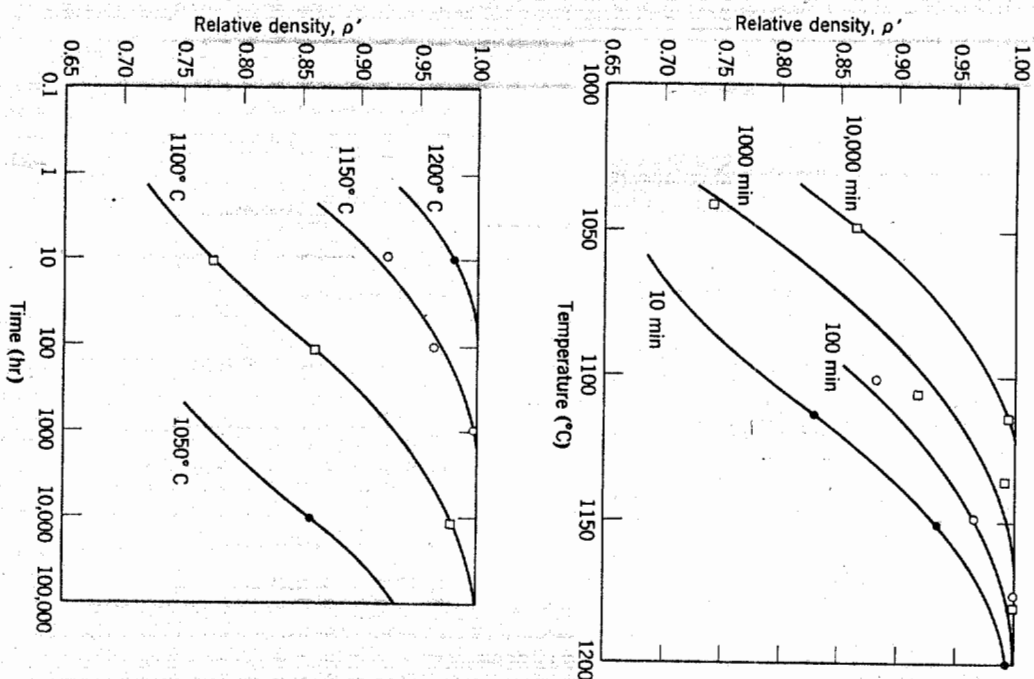


Fig. 10.38. Effect of time and temperature on the vitrification of a porcelain body. Data from F. H. Norton and F. B. Hodgdon, *J. Am. Ceram. Soc.*, 14, 177 (1931).

densification results from longer periods of time at the same temperature. In controlling the process, the temperature dependence is great because of the increase in liquid content and lowered viscosity at higher temperatures. Changes in processing and changes in composition affect the vitrification process as they affect these parameters.

\**J. Am. Ceram. Soc.*, 34, 145 (1951).

### 10.4 Sintering with a Reactive Liquid

Another quite different process which leads to densification is sintering in the presence of a reactive liquid. Here we are referring to systems in which the solid phase shows a certain limited solubility in the liquid at the sintering temperature; the essential part of the sintering process is the solution and reprecipitation of solids to give increased grain size and density. This kind of process occurs in cermet systems such as bonded carbides and also in oxide systems when the liquid phase is fluid and reactive, such as magnesium oxide with a small amount of liquid phase present (Fig. 10.39),  $\text{UO}_2$  with the addition of a small amount of  $\text{TiO}_2$  (Fig. 7.11), and high-alumina bodies which have an alkaline earth silicate as a bonding material.

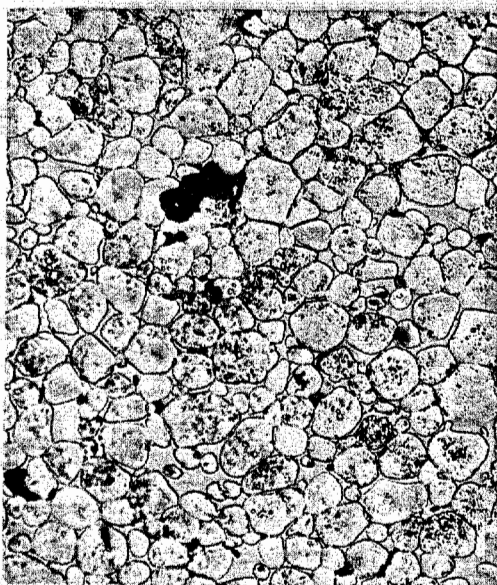


Fig. 10.39. Microstructure of magnesia—2% kaolin body resulting from reactive-liquid sintering (245 $\times$ ).

Studies of a large number of systems indicate that for densification to take place rapidly it is essential to have (1) an appreciable amount of liquid phase, (2) an appreciable solubility of the solid in the liquid, and (3) wetting of the solid by the liquid. The driving force for densification is derived from the capillary pressure of the liquid phase located between the fine solid particles, as illustrated in Fig. 10.40. When the liquid phase wets the solid particles, each interparticle space becomes a capillary in which a substantial capillary pressure is developed. For submicron particle sizes, capillaries with diameters in the range of 0.1 to 1 micron

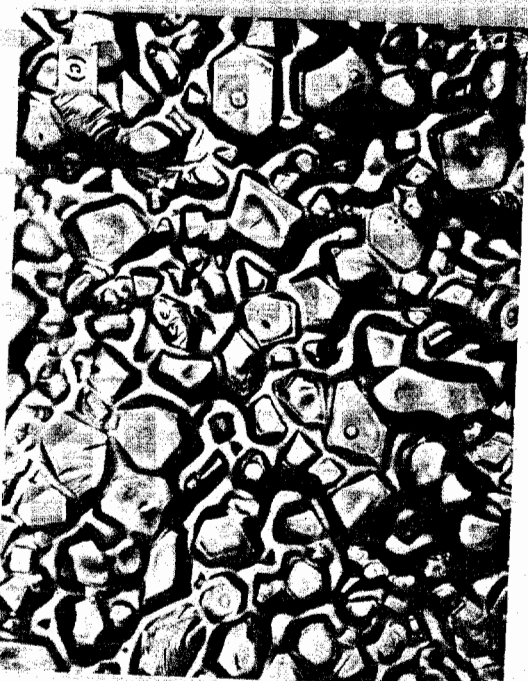
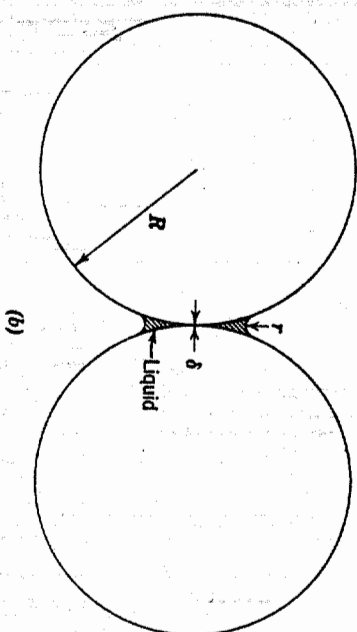
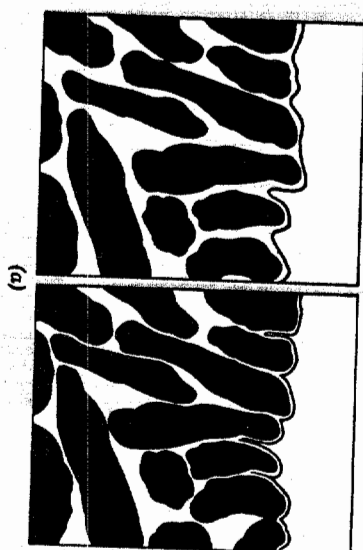


Fig. 10.40. (a) Surface of solid-liquid composite with varying amounts of liquid phase. (b) Drop of liquid between two solid spheres exerts pressure to pull them together. (c) Surface of forsterite ceramic showing liquid capillary depression between crystals.

develop pressures in the range of 175 to 1750 psi for silicate liquids and in the range of 975 to 9750 psi for a metal such as liquid cobalt (see discussion in Chapter 5 and Table 5.2).

The capillary pressure results in densification by different processes which occur coincidentally. First, on formation of a liquid phase there is a rearrangement of particles to give a more effective packing. This process can lead to complete densification if the volume of liquid present is sufficient to fill in the interstices completely. Second, at contact points where there are bridges between particles high local stresses lead to plastic deformation and creep, which allow a further rearrangement. Third, there is during the sintering process a solution of smaller particles and growth of larger particles by material transfer through the liquid phase. The kinetics of this solution-precipitation process have already been discussed in Chapter 9. Because there is a constantly imposed capillary pressure, additional particle rearrangement can occur during grain-growth and grain-shape changes and give further densification. (As discussed for vapor transport and surface diffusion in solid-state sintering, mere solution-precipitation material transfer without the imposed capillary pressure would not give rise to densification). Fourth, in cases in which liquid penetrates between particles the increased pressure at the contact points leads to an increased solubility such that there is material transfer away from the contact areas so that the particle centers approach one another and shrinkage results; the increase in solubility resulting from the contact pressure has been discussed in Chapter 5. Finally, unless there is complete wetting, recrystallization and grain growth sufficient to form a solid skeleton occur, and the densification process is slowed and stopped. Perhaps even more than for the solid-state process, sintering in the presence of a liquid phase is a complex process in which a number of phenomena occur simultaneously. Each has been shown to occur, but experimental systems in which a single process had been isolated and analysed during sintering have not been convincingly demonstrated. Clearly, the process requires a fine-particle solid phase to develop the necessary capillary pressures which are proportional to the inverse capillary diameter. Clearly, the liquid concentration relative to the solid particle packing must be in a range appropriate for developing the necessary capillary pressure. Clearly, if and when a solid skeleton develops by particle coalescence, the process stops.

A critical and still controversial question is the degree of wetting required for the process to proceed. In some important systems such as the tungsten carbide-cobalt and titanium carbide-molybdenum the dihedral angle is zero. In other systems such as iron-copper and magnesia-silicate liquids this is not the case at equilibrium; but the dihedral angle is

low, and the solid is wetted by the liquid phase, as required to develop the necessary capillary pressure. For grain growth of periclase particles in a silicate liquid, the dihedral angle has a large effect on the grain-growth process, as illustrated in Fig. 10.41. Although zero dihedral angle is not essential for liquid-phase sintering to occur, the process becomes more effective as this ideal is approached.

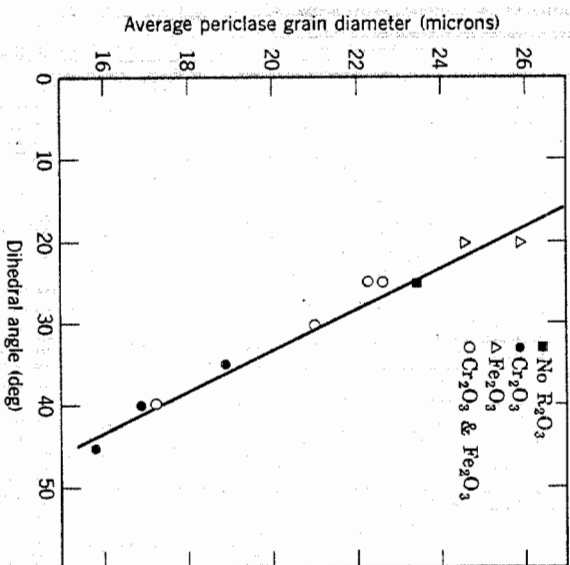


Fig. 10.41. Grain growth of periclase particles in liquid-phase-sintered periclase-silicate compositions as a function of dihedral angle. From B. Jackson, W. F. Ford, and J. White, *Trans. Brit. Ceram. Soc.*, 62, 577 (1963).

### 10.5 Pressure Sintering and Hot Pressing

The sintering processes thus far discussed depend on the capillary pressures resulting from surface energy to provide the driving force for densification. Another method is to apply an external pressure, usually at elevated temperature, rather than relying entirely on capillarity.\* This is desirable in that it eliminates the need for very fine-particle materials and also removes large pores caused by nonuniform mixing. An additional advantage is that in some cases densification can be obtained at a temperature at which extensive grain growth or secondary recrystalliza-

\*R. L. Coble, *J. Appl. Phys.*, 41, 4798 (1970).

tion does not occur. Since the mechanical properties of many ceramic systems are maximized with high density and small grain size, optimum properties can be obtained by hot-pressing techniques. The effect of added pressure on the densification of a beryllium oxide body is illustrated in Fig. 10.42. The main disadvantages of hot pressing for oxide

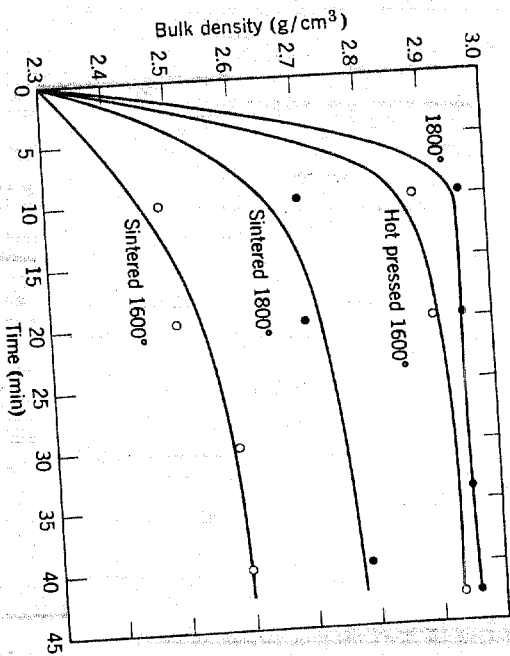


Fig. 10.42. Densification of beryllia by sintering and by hot pressing at 2000 psi.

bodies are the unavailability of inexpensive and long-life dies for high temperatures and the difficulty in making the process into an automatic one to achieve high-speed production. Both factors make the hot-pressing process an expensive one. For oxide materials which have to be pressed at temperature above 1200 or 1300°C (often at 1800 to 2000°C) graphite is the most satisfactory die material available; the maximum stress is limited to a few thousand pounds per square inch, and the life of dies is usually limited to seven or eight pieces. The entire die must be heated and cooled with the formation of each piece. Techniques for using high temperatures in a process in which the die is maintained cool with the material heated have shown some promise in laboratory tests but have not been developed for production.

For lower-temperature materials, such as glasses or glass-bonded compositions which can be pressed in metal dies at temperatures below 800 to 900°C, the hot-pressing process can be developed as an automatic and inexpensive forming method. This is similar to the normal pressing

glass as a glass-forming method in which it is used to obtain the desired shape rather than as a means of eliminating porosity.

Densification during pressure sintering can occur by all the mechanisms which have been discussed for solid-state sintering, vitrification, and liquid-phase sintering. In addition, particularly during the early stages, when high stresses are present at the particle contact points, and for soft materials, such as the alkali halides, plastic deformation is an important densification mode. Since the grain-growth process is insensitive to pressure, pressure-sintering oxides at high pressures and moderate temperatures allows the fabrication of high-density-small-grain samples with optimum mechanical properties and with sufficiently low porosity to be nearly transparent. Covalent materials such as boron carbide, silicon carbide, and silicon nitride can be hot-pressed to nearly complete density. It is often advantageous to add a small fraction of liquid phase (i.e., LiF to MgO, B to silicon carbide, MgO to silicon nitride) to allow pressure-induced liquid phase, or liquid-film, sintering to occur.

### 10.6 Secondary Phenomena

The primary processes which occur on heating and are important in connection with the firing behavior of all ceramic compositions are grain growth and densification, as discussed in previous sections. In addition to these changes, there are a large number of other possible effects which occur during the firing of some particular compositions. These include chemical reactions, oxidation, phase transitions, effects of gas trapped in closed pores, effects of nonuniform mixing, and the application of pressure during heating. Although they are not processes of the most general importance, they frequently cause the main problems and the major phenomena observed during firing. Although we cannot discuss them in great detail, we should at least be familiar with some of the possibilities.

**Oxidation.** Many natural clays contain a few percent organic matter which must be oxidized during firing. In addition, varnishes or resins used as binders, as well as starches and other organic plasticizers, must be oxidized during firing, or difficulties result. Under normal conditions organic materials char at temperatures above 150°C and burn out at temperatures ranging from 300 to 400°C. Particularly with low-firing-temperature compositions, it is necessary to heat at a slow enough rate for this process to be completed before shrinkage becomes substantial. If the carbonaceous material is sealed off from the air by vitrification occurring before oxidation is completed, it acts as a reducing agent at higher temperatures. Sometimes this may merely affect the color, giving rise to

*black coring* of brick and heavy clay products whose interiors are in a reduced state, black in color. A typical example of a stoneware heated too rapidly for oxidation to be completed is illustrated in Fig. 10.43, which shows the central black core. Very often impurities present, particularly sulfides, may cause difficulties unless oxidized before vitrification. Sulfides in general react with oxygen in the temperature range of 350 to 800°C, forming  $\text{SO}_2$  gas which escapes through open pores.



Fig. 10.43. Example of black core produced when time allowed for oxidation reactions was insufficient for completion of the reaction.

In ferrite and titania compositions control of oxidation reactions during firing is particularly important. As illustrated for the  $\text{Ti-TiO}_2$  and  $\text{Fe-O}_2$  systems (Chapter 7), the phases present depend on the oxygen pressure. In addition, as discussed in Chapter 4, the composition of these phases covers a substantial range of stoichiometry and depends on the oxygen pressure. It is common practice in the manufacture of ferrites to control the oxygen pressure during firing so that the composition of each phase present, and the overall phase composition of the body, is maintained to give the best magnetic properties.

**Decomposition Reactions.** Many of the constituents used in ceramic bodies are in the form of carbonates or hydrated compounds; these decompose during firing to form the oxide plus a gaseous product ( $\text{CO}_2$ ,  $\text{H}_2\text{O}$ ). Many impurities are also incorporated as carbonates, hydrates, and sulfates and decompose during firing (see Section 9.4).

Hydrates decompose over a wide temperature range between 100 and 1000°C, depending on the particular composition. Carbonates decompose over a temperature range from 400 to 1000°C, also depending on the particular composition. For each temperature there is, of course, an

equilibrium pressure of the gaseous product; if this pressure is exceeded, further decomposition does not take place, leading to the major problem encountered, the sealing of pores before complete dissociation. As the temperature is raised, the decomposition pressure increases and forms large pores, blistering, and bloating. (This is, of course, the method used to form cellular glass products in which the surface is intentionally sealed off before chemical reaction or decomposition takes place to form a gas phase that expands and produces a foamed product.) This kind of defect is particularly common when high heating rates are used, for then there is a temperature gradient between the surface and interior of the ware, and the surface layer vitrifies, sealing off the interior. This temperature gradient and the time required for oxidation of constituents or impurities are the two most important reasons for limiting the rate of heating during firing.

Sulfates create a particular problem in firing because they do not decompose until a temperature of 1200 to 1300°C is reached. Therefore they remain stable during the firing process used for burning many clay bodies. In particular,  $\text{CaSO}_4$  is stable but slightly soluble in water, so that a high sulfate content leads to a high concentration of soluble salts in the burned brick. This causes efflorescence—the transport of slightly soluble salts to the surface, forming an undesirable white deposit. Addition of barium carbonate prevents the deposit from forming by reacting with calcium sulfate to precipitate insoluble barium sulfate.

Decomposition also occurs in some materials to form new solid phases. A particular example used in refractory technology is the decomposition of kyanite,  $\text{Al}_2\text{O}_3 \cdot \text{SiO}_2$ , to form mullite and silica at a temperature of 1300 to 1450°C. This reaction proceeds with an increase in volume, since both mullite and the silica glass or cristobalite formed have lower densities than kyanite. The reaction is useful, since the addition of kyanite to a composition can counteract a substantial part of the firing shrinkage if the other constituents are carefully selected. Similarly, reaction of  $\text{MgO}$  with  $\text{Al}_2\text{O}_3$  to form spinel occurs with a decrease in volume. By incorporating magnesia and alumina in a refractory mix, or more commonly in a high-temperature ramming mix or cement, the shrinkage taking place on heating can be decreased.

**Phase Transformations.** Polymorphic transformations may be desirable or undesirable, depending on the particular composition and the anticipated use. If a large volume change accompanies the polymorphic transformation, difficulties result, owing to the induced stresses. Refractories cannot be made containing pure zirconium oxide, for example, since the tetragonal monoclinic transformation at about 1000° involves such a large volume change that the ware is disrupted. The source of these

stresses has been discussed in Chapter 5 in connection with boundary stresses caused by differential thermal expansion or contraction of different grains. The expansion or contraction of a crystal in a matrix leads to the same sort of stresses that may give rise to actual cracking, illustrated for quartz grains in a porcelain body in Fig. 10.44. The stresses in individual grains can be reduced if the grain size is reduced; properties of porcelains are improved if fine-grained flint is used rather than coarse material.



Fig. 10.44. Cracked quartz grain and surrounding matrix in a porcelain body. Differential expansion due mainly to the  $\alpha/\beta$  quartz transition leads to cracking of larger grains but leaves small grains intact (500 $\times$ ).

Sometimes desirable phase transformations only occur sluggishly. This is what happens, for example, with the firing of refractory silica brick. The transition from quartz, the starting material, to tridymite and cristobalite, the desired end constituents, occurs only slowly. In order to increase the rate of transformation, calcium oxide is added as a mineralizer. The calcium oxide forms a liquid in which silica is soluble. Consequently the quartz dissolves and precipitates as tridymite, which is the more stable phase (Chapter 7). Some of the quartz transforms directly to cristobalite during the process as well. In general, mineralizers help in achieving equilibrium conditions by providing a mechanism of material transfer—solution or vaporization—that circumvents energy barriers to direct transformations. In silicate systems the addition of fluorides or hydroxyl ions is particularly helpful in this regard, since they greatly increase the fluidity of the liquid phase present.

**Trapped Gases.** In addition to the bloating occasioned by decomposition reactions, trapping of gases within closed pores imposes a limitation

on the ultimate density that can be reached during firing. Gases such as water vapor, hydrogen, and oxygen (to a lesser extent) are able to escape from closed pores by solution and diffusion. In contrast, gases such as carbon monoxide, carbon dioxide, and particularly nitrogen have a lower solubility and do not normally escape from closed pores. If, for example, spherical pores are closed at a total porosity of 10% and a partial pressure of 0.8 atm nitrogen, the pressure has increased to 8 atm (about 110 psi) when they have shrunk to a total porosity of 1%, and further shrinkage is limited. At the same time that the gas pressure is increasing, however, the negative radius of curvature of the pore becomes small so that the negative pressure produced by surface tension is increased proportional to  $1/r$ ; the gas pressure builds up proportional to  $1/r^3$ . For sintering in air this factor usually limits densification; where very high densities are required, as for optical materials or dental porcelains requiring high translucency, vacuum or hydrogen atmosphere is preferred.

**Nonuniform Mixing.** Although not mentioned in most discussions of sintering, the most important reason why densification and shrinkage stop short of complete elimination of pores is that gross defects caused by imperfect mixing and compact consolidation prior to firing are usually present. Examination of typical production ceramics shows that they commonly contain upward of 10% porosity in the millimeter size range (that is, pores much larger than the particle size of the raw materials introduced in the composition). These pores are caused by local variations induced during forming, and there is no tendency for elimination of these pores during firing. Corrective treatment must be taken in the forming method.

**Overfiring.** Ware is commonly referred to as overfired if for any of a variety of reasons a higher firing temperature leads to poorer properties or a reduced shrinkage. For solid-state sintering, such as ferrites and titanates, a common cause is secondary recrystallization occurring at the higher temperature before the elimination of porosity. Consequently, there is some maximum temperature at which the greatest density or optimum properties are obtained. For vitreous ceramics the most common cause of overfiring is the trapping of gases in pores or the evolution of gases which cause bloating or blistering.

### 10.7 Firing Shrinkage

As formed, green ware contains between 25 and 50 vol% porosity. The amount depends on the particle size, particle-size distribution, and forming method (Chapter 1). During the firing process this porosity is removed; the volume firing shrinkage is equal to the pore volume

eliminated. This firing shrinkage can be substantially decreased by addition of nonshrinking material to the mix; fire-clay brick is commonly manufactured with grog (prefired clay) additions which serve to decrease firing shrinkage. Similarly, this is one of the functions of the flint in the porcelain body; it provides a nonshrinking structure which reduces the shrinkage during firing. Terra-cotta compositions, composed of mixtures of fired grog and clay, can be made in large shapes because a large part of the raw material has been prefired and the firing shrinkage is low.

If firing is carried to complete densification, the fractional porosity originally present is equal to the shrinkage taking place during firing. This commonly amounts to as much as 35% volume shrinkage or 12 to 15% linear shrinkage and causes difficulty in maintaining close tolerances. However, the main difficulties are warping or distortion caused by different amounts of firing shrinkage at different parts of the ware. Nonuniform shrinking can sometimes even cause cracks to open.

**Warping.** A major cause of warping during firing is density variations in the green ware. There are many reasons for differences in porosity in the green ware. The density after firing is nearly uniform, and there is higher shrinkage for the parts that had a low density than for the parts that had a high density in the green ware. In pressed ware, pressure variations in the die (Chapter 1) cause different amounts of compaction at different parts of a pressed piece; usually the shrinkage at the center is larger than the shrinkage at the ends, and an hourglass shape results from an initially cylindrical sample (Fig. 10.45a).

Another source of warping during firing is the presence of temperature gradients. If ware is laid on a flat plate and heated from above, there is a temperature difference between the top and bottom of the ware that may cause greater shrinkage at the top than at the bottom and a corresponding warping. In some cases the gravitational stresses may be sufficient to make the ware lie flat, even though shrinkage is nonuniform. The relationship between temperature distribution, warpage, and deformation under the stresses developed is complicated and difficult to analyze quantitatively. Another source of warpage in firing is preferred orientation of the platey clay particles during the forming process. This causes the drying and firing shrinkage to have directional properties.

Vitreous ware is also warped by flow under forces of gravity. This is especially true for large heavy pieces in which substantial stresses are developed. In the forming of vitreous sanitary ware, the upper surface of a closet bowl (Fig. 10.45c) or a lavatory (Fig. 10.45d) must be designed with a greater curvature than is desired in the end product so that the settling which occurs on firing produces a final shape that is satisfactory. A final contributor to warpage during firing is the frictional force or *drag*

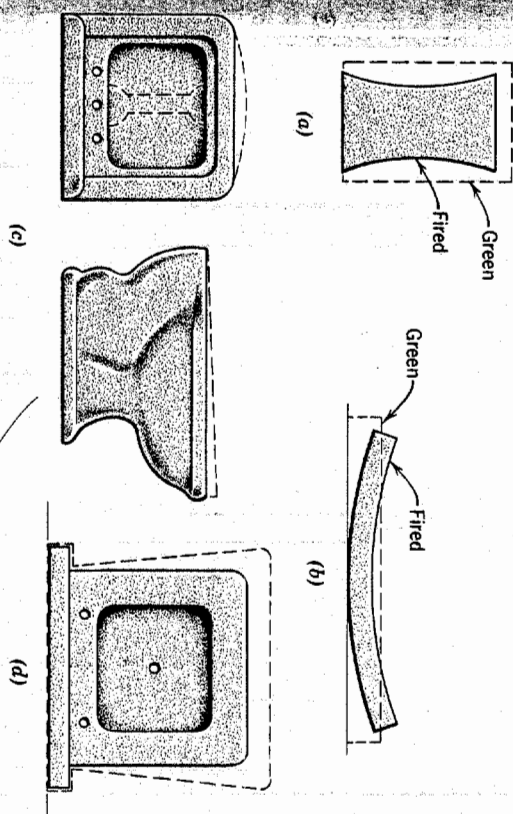
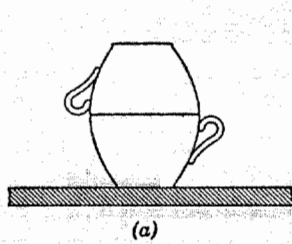


Fig. 10.45. Firing shrinkage of (a) pressed crucible with differential shrinkage due to green density variations, (b) tile with differential shrinkage due to temperature gradients, (c) ware with differential shrinkage due to gravity settling, and (d) differential shrinkage due to frictional force of setting.

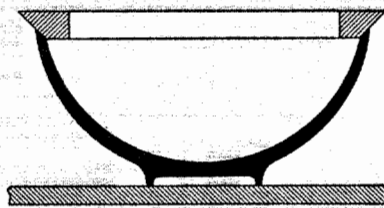
of the ware against the setter. This means that the bottom surface tends to shrink less than the upper surface (Fig. 10.45d). Ware must be designed so that the final shape, including shrinkage, comes out to be rectangular.

Difficulties caused by differential firing shrinkage, resulting distortion, and warping can be eliminated in three ways: first, altering the forming method to minimize the causes of warping; second, designing shapes in a way that compensates for warping; and third, using setting methods in firing that minimize the effects of warping. One obvious improvement in forming methods is to obtain uniformity of the structure during initial forming. This requires elimination of pressure gradients, segregation, and other sources of porosity variation. Pressing samples that have long ratios of length to die diameter cause density variations. Extruded and pressed mixes that have low plasticity are particularly prone to large pressure variations and green density differences. Slip casting and extrusion both cause a degree of segregation and density differences during firing. Some settling may occur during the casting process, causing structural variations. During extrusion pressure differences at various parts of the die or an unsymmetrical setting for the die can cause variations.

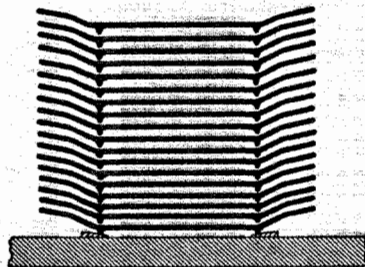
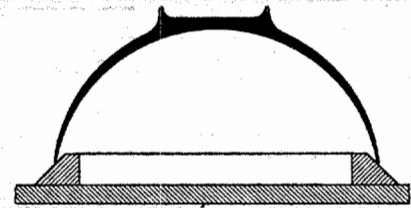
Sometimes variations in firing shrinkage and difficulties from warping can be overcome by compensating the shapes. This is true, for example, in Fig. 10.45, in which the closet bowl and lavatory are designed in such a



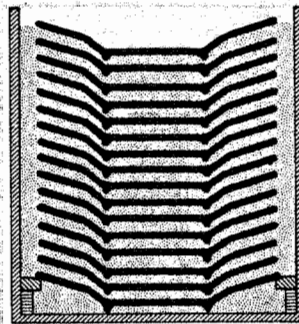
(a)



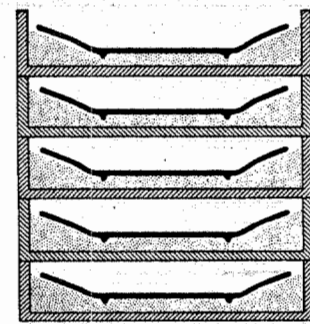
(b)



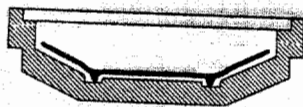
(c)



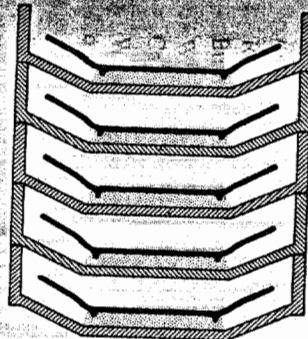
(d)



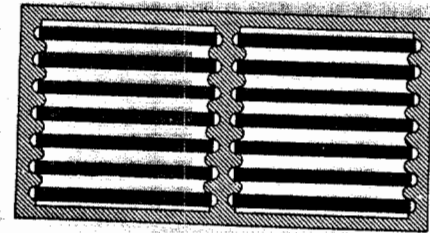
(e)



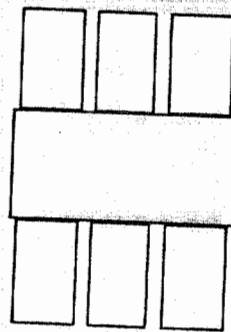
(f)



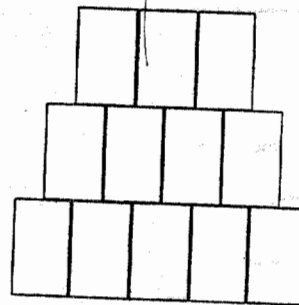
(g)



(h)



(i)



(j)

Fig. 10.46. Setting methods for (a) cups and bowls, (b) large bowls, (c) earthenware, (d) hotel china plates, (e) bone china plates, (f) frit porcelain plates, (g) hard porcelain plates, (h) tile, (i) brick checkerwork, (j) brick bench setting. From F. H. Norton.

way that the final shape is satisfactory. In the same way, when plates are fired in the horizontal position there is a tendency for the rims to settle; this can be compensated for by adjusting the shape of the initial piece.

Correct setting methods are important in eliminating difficulties caused by firing-shrinkage variations. These have been most extensively developed for porcelain compositions in which complete vitrification is desired and high shrinkages result. Some of the standard setting methods are illustrated in Fig. 10.46. Cups and bowls are commonly boxed as indicated in Fig. 10.46a. This keeps the rim circular, since warpage of one restricts warpage of the other; in addition, it prevents the thin rims from being too rapidly heated. For larger pieces, unfired setters are necessary as a means of controlling shrinkage and maintaining circular rims. A variety of methods is used for setting different kinds of plate compositions, depending on the amount of shrinkage expected. For ware fired to complete vitrification individual setting and support are essential. For ware fired to partial densification, plates can be stacked with no ill effects. In general, large tiles and brick do not cause much difficulty.

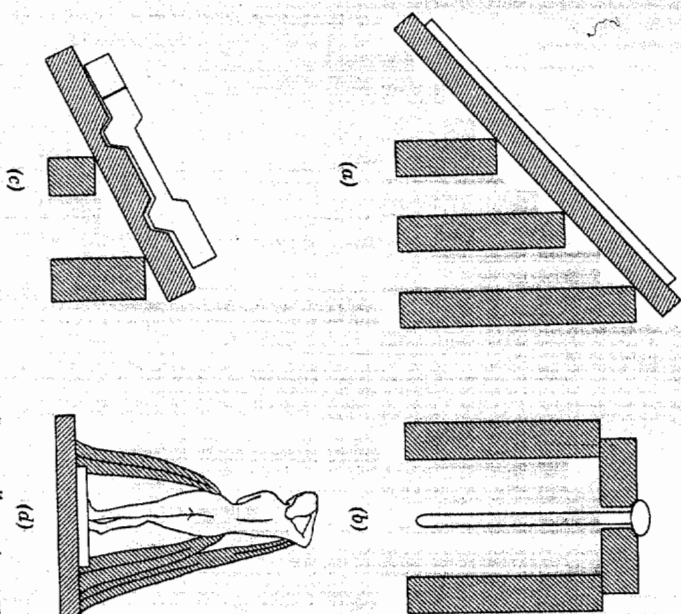


Fig. 10.47. Setting methods for special shapes. (a) Large tiles set at an angle of repose; (b) slender rod supported by collar; (c) special shape; (d) sculptured piece. From F. H. Norton.

Special shapes may require special setting methods to eliminate adverse effects of firing shrinkage. Large refractory tile can be set at an angle of repose on a flat surface (Fig. 10.47a). This allows the tile to shrink without much stress. In the same way rods or tubes may be set in an inclined V groove or supported by a collar from the upper end (Fig. 10.47b). Gravitational forces keep the tubes straight up to lengths of several feet. Unique shapes can always be supported on special setters designed for the particular sample. Some experience is necessary to handle unique shapes efficiently. Small pieces of sculptured vitrified ware are particularly difficult. The safest setting provides complete support from unfired struts (Fig. 10.47d).

### Suggested Reading

1. G. C. Kuczynski, N. A. Hooton, and C. F. Gibson, Eds., *Sintering and Related Phenomena*, Gordon and Breach, New York, 1967.
2. G. C. Kuczynski, Ed., "Sintering and Related Phenomena", *Materials Science Research*, Vol. 6, Plenum Press, New York, 1973.
3. R. L. Coble and J. E. Burke, *Progress in Ceramic Science*, Vol. III, J. E. Burke, Ed., Pergamon Press, 1963.
4. W. D. Kingery, Ed., *Ceramic Fabrication Process*, Part IV, Technology Press, Cambridge, Mass., and John Wiley & Sons, New York, 1958.
5. W. D. Kingery, Ed., *Kinetics of High-Temperature Process*, Part IV, Technology Press, Cambridge, Mass., and John Wiley & Sons, New York, 1959.
6. J. E. Burke and D. Turnbull, "Recrystallization and Grain Growth in Metals," *Prog. Met. Phys.*, **3**, 220 (1952).
7. E. Schramm and F. P. Hall, "The Fluxing Effect of Feldspar in Whiteware Bodies," *J. Am. Ceram. Soc.*, **15**, 159 (1936).
8. For additional papers on sintering see: R. L. Coble, *J. Appl. Phys.*, **41**, 4798 (1970); D. L. Johnson and I. B. Cutler, *J. Am. Ceram. Soc.*, **46**, 541 (1963).

### Problems

- 10.1. Distinguish between primary recrystallization, grain growth, and secondary recrystallization as to (a) source of driving force, (b) magnitude of driving force, and (c) importance in ceramic systems.
- 10.2. Explain why the activation energy for grain-boundary migration corresponds approximately with that for boundary diffusion, even though no concentration gradient exists in the former case.
- 10.3. Can grain growth during sintering cause compaction of ceramics? Explain. Can grain growth affect the sintering rate? Explain.

- 10.4. Which of the following processes can contribute increased strength to sintered articles without causing compaction? Explain.

- (a) Evaporation condensation.
- (b) Volume diffusion.
- (c) Viscous flow.
- (d) Surface diffusion.
- (e) Solution reprecipitation.

- 10.5. Assuming the surface energy of  $\text{NiCr}_2\text{O}_4$  is  $600 \text{ erg/cm}^2$  and estimating diffusion data from  $\text{Cr}_2\text{O}_3$  and  $\text{NiO}$  data given in Chapter 6, what would be the initial rate of densification for a compact of 1-micron particles at  $1300^\circ\text{C}$ ? at  $1400^\circ\text{C}$ ? at  $1200^\circ\text{C}$ ?

- 10.6. If pores of 5-micron diameter are sealed off containing nitrogen at a pressure of 0.8 atm in a glass having a surface tension of  $280 \text{ dyne/cm}$  and a relative density of 0.85, what will be the pore size at which the gas pressure just balances the negative pressure due to the surface tension? What will be the relative density at this point?

- 10.7. Explain the mechanism of reactive-liquid sintering, such as occurs for Co-WC compositions. Identify two critical solid-liquid interaction characteristics in a system showing this behavior, and describe how you would quantitatively measure them.

- 10.8. From data collected during sintering of powder compacts of nominally pure simple phase materials at variable heating rates, the observed rates of density change analyzed on an Arrhenius plot frequently give activation energies higher in value than that for lattice self-diffusion. There are three sets of assumptions on which this behavior can be rationalized. Give two examples of suitable assumptions, and explain the behavior on a mechanistic basis.

- 10.9. During the normal grain growth of  $\text{MgO}$  at  $1500^\circ\text{C}$ , crystals were observed to grow from 1 micron diameter to 10 micron diameter in 1 hr. Knowing that the grain boundary diffusion energy is  $60 \text{ kcal/mole}$ , predict the grain size after 4 hr at  $1600^\circ\text{C}$ . What effect would you predict impurities will have on the rate of grain growth of  $\text{MgO}$ ? Why?

- 10.10. Suppose that in order to reduce sintering shrinkage you were to mix enough fine particles (about 30%), 1 micron in diameter, with coarse particles, 50 microns in diameter, so that all the interstices between the coarse particles were filled with fine particles. What would be the rate of shrinkage of this compact? Make a plot of  $\log(\Delta L/L_0)$  versus  $\log t$ , and place the 1-micron powder and 50-micron powder shrinkage lines in their relative positions; then place the shrinkage curves for the composite material in its proper position with respect to the 1-micron and 50-micron curves. Justify your answer.

- 10.11. A certain magnetic oxide material is believed to follow the normal grain-growth equation. Magnetic-strength properties deteriorate when grain size increases beyond an average of 1 micron. The original grain size before sintering is 0.1 micron. Sintering for 30 min triples the grain size. Because of warping of large pieces, the superintendent of production wants to increase the sintering time. What is the maximum time you would recommend?

- 10.12. Alumina with  $\text{MgO}$  is sintered to nearly theoretical density in hydrogen to the point that the optical transmission in the visible range is almost 100%. Actually the material (Lucalox) is not transparent but translucent because of the hexagonal crystal structure of alpha alumina. It is used to contain sodium vapor (at pressures above atmospheric) for street lamps. An alternative candidate for this application is

$\text{CaO}$  which is cubic and could be transparent if sintered to theoretical density. Outline your research program if you were to seek to make  $\text{CaO}$  transparent through sintering.

10.13. The time required to shrink 5% for a compact of 30-micron glass spheres is 209.5 min at  $637^\circ\text{C}$  and 5.8 min at  $697^\circ\text{C}$ . Compute the activation energy and viscosity of the glass on the basis that surface energy is  $300 \text{ ergs/cm}^2$ .